# Modeling Nontraumatic Aneurysm Evolution, Growth and Rupture

Tor A. Kwembe[*] and Ashley M. Sanders

*Department of Mathematics and Statistical Sciences, Jackson State University, JSU Box 17610, Jackson, MS 39217, USA*

**Abstract:** We have presented a mathematical model to study the evolution, growth and risk rupture of nontraumatic aneurysms contained within a cylindrical region of blood vessels. Analytical and numerical solutions are studied. Results affirmed that the intra-aneurysmal pressure and bloodstream flow account for the evolution and growth of aneurysms, and we find that an aneurysm may rupture when the ratio of the lateral membrane contraction to longitudinal membrane extension approaches one. Numerical properties of intra-aneurysmal pressure, impact fluid velocity, membrane displacement and the deformed radius with respect to the Poisson ratio, membrane thickness and extensional rigidity are studied. The importance of the findings is rested on the fact that they can be used to improve noninvasive means for predicting aneurysm rupture, and treatment and management decisions after rupture.

## 1. INTRODUCTION

In this paper, we describe a mathematical model which may lead to understanding the evolution, growth and rupture potential of nontraumatic aneurysms. The model describes a quasi-static, non-convectional acceleration, axi-symmetric Navier-Stokes equations in cylindrical coordinates coupled with the Camenschi-Fung [1, 2] type linear elastodynamic system of equations with filtration. The profile of solutions of the system of equations described may help to provide insights in developing noninvasive means for detecting when a nontraumatic aneurysm may rupture and deciding the best treatment and management strategies of ruptured aneurysms.

The genesis of a nontraumatic aneurysm is contingent on any condition that causes the walls of the blood vessel to weaken [3-8]. The most commonly investigated forms of aneurysms are the aortic, cerebral artery and intracranial aneurysm[3, 5-7, 9-11]. The development of the cerebral aneurysm, for example, is contingent on various physical factors associated with blood flow [3, 5, 10]. Studies suggest that the inertial forces of the bloodstream result in the local elevation of intravascular pressure and the flow impact [9]. This means that, the impacting forces and the local pressure elevation at the aneurysm have a large contribution to the development of cerebral aneurysms. The other contingent factor is the wall shear stress, which is the viscous friction of the bloodstream that acts parallel to the vessel wall [3, 9, 12]. The overall impact of these forces on the thinning of the aneurysm wall has not been suggested in the literature. In this study, we have shown that when the lateral contraction of the membrane wall is in balance with the longitudinal extension, an aneurysm may rupture and that at the rupture point about 80% of the membrane wall thins out. The analytical and numerical results presented here affirms the results in the literature [3, 9, 10] that the intra-aneurysmal pressure and the bloodstream flow contribute to the evolution and development of aneurysms.

Modern neuroimaging techniques often detect unruptured cerebral artery aneurysm, which is estimated to be present in 3%-6% of the population [9, 10]. Aggressive rupture preventing treatment is often an option, but may lead to morbidity. The specific risk for rupture of a nontraumatic aneurysm is unknown and risk assessments are based on general knowledge of factors leading to subarachnoid hemorrhage deduced from epidemiological studies [6, 9, 10]. Additionally, aneurysms of large size, proximal location, and small neck, or fundus ratio are associated with increased risk for rupture [5, 9, 10]. Thus, more reliable parameters to predict the risk of aneurysmal rupture are needed. Intra-aneurysmal pressure gradients, bloodstream flow profiles, membrane displacement profiles, membrane thickness, and Poisson ratio could provide additional information regarding the risk of rupture. Moftakher, R. *et al.* hypothesized in [13] that Phase Contrast with vastly undersampled isotropic projection reconstruction could accurately assess intra-aneurysmal pressure gradients in a canine aneurysmal model when compared with invasive measurements. Isaken, J. G. *et al.* developed in [9] a computational model for simulation of fluid-structured interaction in cerebral

*Address correspondence to this author at the Department of Mathematics and Statistical Sciences, Jackson State University, JSU Box 17610, Jackson, MS 39217, USA; Tel: 601-979-2161; Fax: 601-979-5852; E-mail: tor.a.kwembe@jsums.edu

aneurysms based on patient specific lesion geometry, with emphasis on wall tension.

In the proposed model, we have introduced additional parameters, the Poisson ratio and membrane wall thickness, as determining measures predicting the potential for an aneurysm to rupture. The mathematical model is constituted by equations (1) - (14) of section 2. We used the Camenschi dimensionless variable transforms and quasi-static conditions [1] to reduce the problem to parameters that can be measured by noninvasive means. The analytical solutions provide conditions for membrane enlargement to minimum and maximum stretches that depends on the intra-aneurysmal pressure gradients and rates. It also reveals that a nontraumatic aneurysm may rupture when the Poisson ratio, $v_0$, approaches anisotropic material values. In section 3, we provide numerical analysis of the solutions based on experimental data of parameters derived from the cited literature. The analysis confirms that the profile of the deformed radius and the displacement components of the membrane becomes discontinuous as the Poisson ratio approaches anisotropic material values. Numerical analysis of intra-aneurysmal pressure, membrane displacement and thickness affirm that their profile before and after the rupture of an aneurysm are consistent with *in vitro* and *in vivo* observations. In particular, it shows that when 80% of the membrane wall thins out then the aneurysm may rupture.

There are many hypotheses regarding aneurysm enlargement and rupture [3-10]. However, the roles of the Poisson ratio and the thinning of the membrane wall are not well understood. Shah and Humphrey suggested in [14] that studies on the mechanics of saccular aneurysms should be focused on quasi-static analyses that investigate the roles of lesion geometry and material properties including growth and remodeling. The model presented here has taken the material properties, growth and remodeling into account. Remodeling of the membrane wall in responses to tears is incorporated in the filtration coefficient and retain the normal balance in the micro-vascular mechanism in supplying tissues or the surrounding fluids with nutrients and clearing waste products. However, the model does not take into consideration the healing process of the membrane layers. Another interesting finding is that when the Poisson ratio is in the range $0 \leq v_0 < 1$, and $v_0 > 2$, the aneurysm may stretch or shrink but not rupture. In fact, most experimental studies choose values of Poisson ratio in the isotropic material range $0 < v_0 < 0.5$ and do not factor the filtration process and anisotropic material composition of the membrane's inner and outer layers,

which remain in place after the media has deflated (aneurysm has ruptured), into consideration. We have considered the Poisson ratio in the anisotropic material range $1 < v_0 < 2$ in this study to indicate that the membrane extensional rigidity is weakened by generating a substantial anisotropy in stiffness. This is discussed in section 2 in the activities leading to the development of an aneurysm sac in the media layer of the membrane which is surrounded by the inner and outer layers made of dominantly polyurethane material which is anisotropic [15]. In section 4, we provided the post rupture analysis and demonstrated how the membrane extensional rigidity deduced from the membrane wall thickness and Poisson ratio can be used to design a grading scale to measure the severity of aneurysm rupture.

## 2. MATHEMATICAL MODEL

We will derive a model and then illustrate how it can be used to model the evolution, growth, and predict the rupture potential of nontraumatic aneurysms. It is known that inertial forces of the bloodstream results in local elevation of intra-vascular pressure and the flow impacting force together with local pressure elevation at the aneurysm contributes to the development of aneurysms [10, 12]. It is also hypothesized that aneurysms rupture when the wall tension exceeds the strength of the wall tissue. We shall consider an axi-symmetric motion of equation in two media; the Newtonian fluid, coupled with the linear elastic membrane. Due to the nature of the origin of the blood flow into the blood vessels, which is imposed by the heart pumping blood into the circulatory system, we shall consider non-convection acceleration, axi-symmetric, viscous, incompressible pressure driven Navier-Stokes equations in cylindrical coordinates coupled with the Camenschi-Fung type elastic membrane equations [1, 2, 16]. We shall assume that the aneurysm occurs within a cylindrical portion of the vessel of length $L$. We let $a_0$ be the undeformed radius of the cylinder and $a(z,t)$ be the deformed radius describing the curvature of the aneurysm. We let $P(z,t)$ be the intra-aneurysmal pressure with $P_1(t)$ and $P_2(t)$ the end pressures at $z = 0$ and $z = L$ respectively (See Figure **1**).

If we let $\bar{v} = (v,u)$ be the velocity vector of the fluid flowing through the portion of the vessel containing the aneurysms where $v(z,r,t)$ and $u(z,r,t)$ are the transversal and longitudinal components, and $\bar{\eta} = (\xi,\zeta)$ is the displacement vector of the membrane. $\xi(z,t)$ and $\zeta(z,t)$ are the transversal and longitudinal components of the membrane displacement respectively as illustrated in Figure **1** and furthermore,
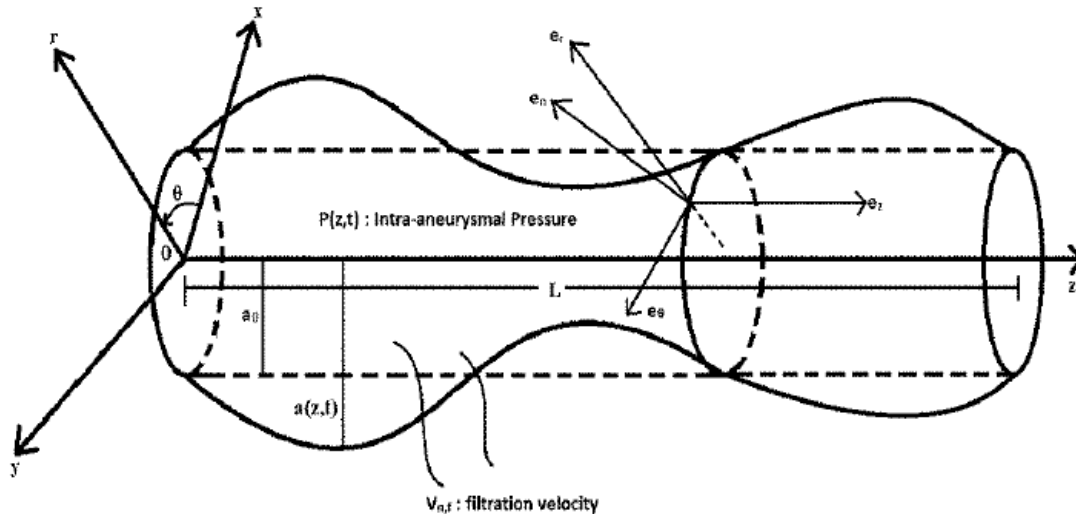
**Figure 1:** Model of a deformed membrane contained within a cylindrical portion of a blood vessel.

if $t_{rz}$ and $t_{rr}$ are the stress tensor components in the fluid then, we have the Camenschi-Fung type system of equations [1, 2]:

$$\frac{\partial v}{\partial t} = -\frac{1}{\rho}\frac{\partial P}{\partial r} + \frac{\mu}{\rho}\left[\frac{\partial^2 v}{\partial r^2} + \frac{1}{r}\frac{\partial v}{\partial r} + \frac{\partial^2 v}{\partial z^2} - \frac{v}{r^2}\right]; \tag{1}$$

$$\frac{\partial u}{\partial t} = -\frac{1}{\rho}\frac{\partial P}{\partial r} + \frac{\mu}{\rho}\left[\frac{\partial^2 u}{\partial r^2} + \frac{1}{r}\frac{\partial u}{\partial r} + \frac{\partial^2 u}{\partial z^2}\right]; \tag{2}$$

$$\frac{\partial v}{\partial r} + \frac{v}{r} + \frac{\partial u}{\partial z} = 0 \tag{3}$$

$$\rho_m h \frac{\partial^2 \zeta}{\partial t^2} = D\left(\frac{v_0}{a_0}\frac{\partial \xi}{\partial z} + \frac{\partial^2 \zeta}{\partial z^2}\right) + t_{rz}\big|r = a_0; \tag{4}$$

$$\rho_m h \frac{\partial^2 \xi}{\partial t^2} = -D\left(\frac{v_0}{a_0}\frac{\partial \zeta}{\partial z} + \frac{\xi}{a_0^2}\right) - t_{rr}\big|r = a_0; \tag{5}$$

$$t_{rz} = -\mu\left(\frac{\partial u}{\partial r} + \frac{\partial v}{\partial z}\right)\big|r = a_0 \tag{6}$$

$$t_{rr} = \left(P - 2\mu\frac{\partial u}{\partial r}\right)\big|r = a_0 \tag{7}$$

defined in the region $0 < r \le a_0 \le a(z,t); 0 < z < L; t \ge 0$ where $\rho$ is the mass density of the fluid, $\mu$ is the dynamic viscosity, $\rho_m$ is the mass density of the membrane, $h$ is the thickness of the membrane wall, $D = \dfrac{Eh}{1-v_0^2}$ is the extensional rigidity of the membrane, $E$ is the Young's modulus, and $v_0$ is the Poisson ratio.

A normal artery wall consist of three layers. The innermost endothelial layer is called the intima, the middle layer consisting of smooth muscle is called the media and the other layer consisting of connecting tissues is called the adventitia [2]. The deformed curvature of the blood vessel or aneurysmal sac is composed of only the intima and adventitia. The material composition of the intima and adventitia is made up of dominantly anisotropic polyurethane. The intima, based on *in vitro* and *in vivo* observations [17, 18] remains normal but subintimal cellular proliferation also occurs when aneurysm developed. The internal elastic membrane responsible for the thinning of the artery wall is either reduced in size or absent causing the media to retract to the junction of the aneurysm neck with the parent blood vessel. This development transforms the membrane within the aneurysm region from pseudoelastic isotropic to anisotropic media. Thus, the deformation transforms the curvature of the weakened portion of the blood vessel into an aneurysmal sac and hence tolerating the extension of the membrane and transverse shear, curving and pressure difference. We shall consider the blood vessels as permeating deformable shell filled with a pulsating incompressible fluid and constrained by the surrounding tissue and fluid. The extensional rigidity D of the membrane depend on its stiffness and the deformation grows in the direction of the space created by the surrounding tissue due to impacting forces on the vessel wall. The deformation of the vessel is not volume preserving but the biological material properties of the membrane are more or less the same everywhere and transition from isotropic to anisotropic media as aneurysm evolved. It is also biologically known that the interior of a cell is anisotropic due to intracellular organelles. This characteristic may be responsible for the development of two or more aneurysms on the same artery. Multiple aneurysms are due to defects in the arterial wall and may be

congenital [19]. Nevertheless, we shall consider the membrane as a pseudoelastic isotropic material in the biological sense [2] that the material properties of the membrane remain the same throughout the deformation process becoming anisotropic only during the development of aneurysm sac. This feature holds only for nontraumatic aneurysms. The theory of isotropic elasticity allows the Poisson ratio in the range $-1 \le v_0 \le 0.5$ for an object with surface with no constraint. Physically, this means that for the material to be stable, the stiffness must be positive. That is, it is required that both the bulk and shear modulus be greater than or equal to zero [20, 21]. On the other hand, isotropic objects that are constrained at the surface can have Poisson ratios outside the above range and be stable [20, 21]. Since the blood vessels are constrained by the surrounding tissue and fluid, we shall consider values of Poisson ratio to include values outside the isotropic range $-1 \le v_0 \le 0.5$. This consideration also includes the regime of anisotropic deformation, when the constituted material of the membrane within the aneurysm region is made up of the intima and adventitia, since the concept of Poisson ratio can be extended to anisotropic materials with values outside the isotropic range $-1 \le v_0 \le 0.5$ [15, 20-23].

We shall also assume that the natural vascular process of exchange of nutrients and waste from the evolution and development of aneurysms are by filtration. Thus, the boundary conditions expressing the adherence of the fluid to the membrane wall and the fluid filtration through the membrane are:

$$v(z,a(z,t),t) = \frac{\partial \xi}{\partial t} + \frac{v_{n,f}}{\sqrt{1+\left(\frac{\partial a}{\partial z}\right)^2}} \qquad (8)$$

$$u(z,a(z,t),t) = \frac{\partial \zeta}{\partial t} + \frac{v_{n,f}\left(\frac{\partial a}{\partial z}\right)}{\sqrt{1+\left(\frac{\partial a}{\partial z}\right)^2}^*} \qquad (9)$$

where $v_{nf}$ is the filtration velocity normal to the membrane wall, and we supposed that it is governed by the Darcy-Starling Law [14, 24] given as:

$$v_{n,f} = \frac{k^*}{\mu h}(P(z,t) - P_e) \qquad (10)$$

where $k^*$ is the permeability coefficient and $P_e$ is the constant exterior pressure.

We will now justify (10). In a normal vascular system of functions, there is a free exchange of nutrients, water, electrolytes and microphage between the intra-vascular and extra-vascular components of the blood vessels. Several mechanisms are responsible for this critical function of the vascular system. Physiologists, including Michel [12, 25, 26] investigated the mechanism by which plasma and its solutes cross the vascular barrier. They discovered that capillaries are the vascular segment responsible for molecular exchange in normal tissues and that gases, water and microphages cross the capillary endothelial cell barrier freely, but the passage of larger molecules such as plasma proteins are tightly restricted. They also discovered that several mechanisms are involved in this exchange. The most important, though, are the bulk flow and diffusion. The rate of change in either direction is determined by physical factors such as hydrostatic pressure, osmotic pressure, and the physical nature of the barrier separating the blood and the interstitium of the tissue. That is, the permeability of the membrane wall. While the diffusion process is deemed the most important mechanism in this exchange, the diffusion coefficient in the Fick equation [27] depends on molecular size [28]. It is important for the exchange of small molecules which is driven by molecular concentration gradient across vascular endothelium defined by the Fick equation $J_0 = k(C_v - C_i)$. $C_v - C_i$, is the concentration difference. Sample and Golovin employed this condition in [29, 30] to study the dynamics of a double-lipid bilayer membrane by coupling intermembrane separation and the lipid chemical composition of a two-component membrane and dependence on the membrane curvatures. They focused on the thermodynamical equilibrium in [29] and non-equilibrium in [30] of fluxes across the membrane. In this derivation, we are considering the impacting forces on the membrane, rather than the concentration of the fluid content of the blood vessels and hence admit the exchange of large molecular fluxes, such as plasma proteins. Consequently, filtration is much more important than diffusion for flux of large molecules such as plasma proteins and is governed by the Starling equation [12, 13, 25, 26]:

$$v_{nf} = \frac{k^*}{\mu h}\left[\left(P(z,t) - P_e\right) - \sigma\left(\pi - \pi_e\right)\right],$$

where $k^*$, the filtration coefficient, is a property of the membrane wall and a measure of the permeability of the membrane to water, $P - P_e$ and $\pi - \pi_e$ are hydrostatic and osmotic pressure differences, respectively, between the plasma and the interstitium, $\sigma$ is the osmotic reflection coefficient and varies from zero to one. High values of $\sigma$ indicate little plasma-protein escape [28]. When $\left(P(z,t) - P_e\right) - \sigma\left(\pi - \pi_e\right)$ is

positive, filtration takes place and when it is negative reabsorption takes place. The amount of fluid filtered or reabsorbed per unit time, the filtration velocity or flux is determined by the permeability of the membrane and by the surface area available for the exchange.

Vascular permeability is essential for the health of normal tissues and it is also an important characteristic of many disease state in which it is greatly increased [12, 25, 26, 28]. Since aneurysm is caused by the weakening of the membrane which results in high levels of plasma-protein escape activity, we shall take the osmotic reflection coefficient to be zero and, therefore, arrive at the Darcy-Starling filtration velocity given in equation (10). That is, when an aneurysm evolved, the reabsorption process is stopped.

The values of the pressure at the ends of the aneurysm region are given by:

$$P(0,0,t) = P_1(t); \quad P(L,0,t) = P_2(t). \tag{11}$$

We further assume that, the end at $z = 0$, the beginning of the aneurysm region is fixed and the end of the aneurysm region $z = L$ is free of stress, we have:

$$\zeta\big|_{z=0} = 0; \quad D\left(\frac{\partial \zeta}{\partial z} + v_0 \frac{\xi}{a_0}\right)\bigg|_{z=L} = 0; t \geq 0 \tag{12}$$

The deformed radius is given by

$$a(z,t) = a_0 + \xi(z,t); \quad 0 < z < L; \quad t \geq 0. \tag{13}$$

We further make the following assumptions: (1) the length $L$ of the aneurysm region must be much larger than the undeformed radius of the blood vessel and (2):

$$\left(\frac{a_0}{L}\right)^2 \ll 1; \quad \frac{\rho u_* a_0}{\mu} \ll 1; \quad \frac{\rho_m h u_*^2}{D} \ll 1. \tag{14}$$

where $u_*$ is the characteristic longitudinal speed.

Thus, equations (1) - (14) constitute the mathematical model describing the evolution and development of aneurysms contained within a cylindrical portion of the blood vessel. If any form of aneurysm occurs within the cylindrical portion of the arteries or blood vessels, in general, then the deformed radius $a(z,t)$ defines the geometry of the aneurysm. Since, as Figure **1** shows, the extension, or stretch, of $a(z,t)$ is measured through the neck of the aneurysm, or the opening into the aneurysm (fundus aspect ratio), from the bloodstream vessel. Consequently, the model given here can be used to study the characteristics of all forms of aneurysms within a cylindrical portion of the vessel.

Assumption 2 in (14) leads to a quasi-static problem. That is, initial conditions are not needed to solve and analyze the problems of aneurysm evolution and development. We now non-dimensionalize equations (1) - (13) using (14) and the following Camenschi [1] dimensionless variable transformations

$$t = \frac{L}{u_*} t^0; \quad z = L z^0; \quad r = a_0 r^0; v = \frac{u_* a_0}{L} v^0; u = u_* u^0;$$

$$P = \frac{\mu u_* L}{a_0^2} P^0; \zeta = \varepsilon L \zeta^0; \quad \xi = \varepsilon a_0 \xi^0; a(z,t) = a_0 a^0(z^0, t^0)$$

where $\varepsilon < 1$ is a dimensionless parameter given as

$$\varepsilon = \frac{P_* a_0}{D} = \frac{\mu u_* L}{a_0 D}.$$

The expression for $\varepsilon$ and condition (14) are natural scaling obtained from the nondimensional analysis process and agreed with those of fluid flow in permeable media and Camenschi [1]. The superscript index "0" is used for dimensionless quantities. Upon dropping the index after transformation, equations (1) - (13) reduces to the following dimensionless equivalent equations:

$$\frac{\partial P}{\partial r} = 0; \quad 0 < r \leq 1 \leq a(z,t); \quad t \geq 0 \tag{15}$$

$$\frac{\partial P}{\partial z} = \frac{1}{r} \frac{\partial}{\partial r}\left(r \frac{\partial u}{\partial r}\right); \quad 0 < r \leq 1 \leq a(z,t); \quad 0 < z < 1; t \geq 0 \tag{16}$$

$$\frac{1}{r} \frac{\partial}{\partial r}(rv) + \frac{\partial u}{\partial z} = 0; \quad 0 < r \leq a_0 \leq a(z,t); \quad 0 < z < 1 \tag{17}$$

$$v_0 \frac{\partial \xi}{\partial z} + \frac{\partial^2 \zeta}{\partial z^2} = \frac{\partial u}{\partial r}\big|r = 1; \quad 0 \leq z \leq 1 \tag{18}$$

$$v_0 \frac{\partial \zeta}{\partial z} + \xi = P(z,t); \quad 0 \leq z \leq 1; \quad t \geq 0 \tag{19}$$

along with the boundary conditions:

$$v(z,r,t)\big|_{r=a(z,t)} = \varepsilon \frac{\partial \xi}{\partial t} + \delta(P - P_e); \quad 0 \leq z \leq 1; \quad t \geq 0 \tag{20}$$

where $\delta = \frac{k^* L^2}{h a_0^3}.$

$$u(z,r,t)\big|_{r=a(z,t)} = \varepsilon \frac{\partial \zeta}{\partial t}; \quad t \geq 0; \quad 0 \leq z \leq 1 \tag{21}$$

$$\zeta\big|_{z=0} = 0; t \geq 0 \tag{22}$$

$$\varepsilon\left(\frac{\partial \zeta}{\partial z} + v_0 \xi\right)\bigg|_{z=1} = 0; t \geq 0 \tag{23}$$

$$P(0,t) = P_1(t); \quad P(1,t) = P_2(t); \quad t \geq 0 \tag{24}$$

$$a(z,t) = 1 + \varepsilon\xi(z,t); \quad 0 \leq z \leq 1; \quad t \geq 0. \tag{25}$$

We note here that the dimensionless system of equations constitute only the intra-vascular pressure, the components of the fluid velocity and membrane displacement, the Poisson ratio $v_0$ and the filtration coefficient $k^*$ as the inertial forces impacting the membrane wall. Since in simulation, $\varepsilon$ will always be taken to be less than one, the mass densities and fluid viscosity do not play a major role in the evolution and development of an aneurysm and in its potential to rupture. In dimensionless analysis, the evolution of an aneurysm will always depend on the size of the transversal displacement of the membrane and wall thickness, $h$.

We also note that the dimensionless equations of the non-convection acceleration Navier-Stokes equations are the same as with the Camenschi's convection acceleration, quasi-static equations. Thus, making the mathematical model given here a slow flow, quasi-static problem. The solutions to the system of equations (15) - (24) as with Camenschi in [1] are obtained by direct integration under the conditions that $v(z,r,t)$ and $u(z,r,t)$ remain bounded at $r = 0$ and noting from equation (15) that $P = P(z, r, t)$ only. Hence, we have the following expression for the fluid velocity and membrane displacement components. The argument *(z, r, t)* is omitted in $P$, $\xi$, and $\zeta$ in some cases for printing convenience.

$$v(z,r,t) = \left[\frac{-r^3}{16} + \frac{r}{8}(1+\varepsilon\xi)^2\right]\frac{\partial^2 P}{\partial z^2} + \frac{\varepsilon r}{4}(1+\varepsilon\xi)\frac{\partial \xi}{\partial z}\frac{\partial P}{\partial z} - \frac{\varepsilon r}{2}\frac{\partial^2 \zeta}{\partial z \partial t} \tag{26}$$

$$u(z,r,t) = \frac{1}{4}[r^2 - (1+\varepsilon\xi(z,t))^2]\frac{\partial P(z,t)}{\partial z} + \varepsilon\frac{\partial \zeta(z,t)}{\partial t} \tag{27}$$

$$\xi(z,t) = \frac{2-v_0}{2(1-v_0^2)}P(z,t) + \frac{v_0}{2(1-v_0^2)}P_2(t) \tag{28}$$

$$\zeta(z,t) = \frac{1-2v_0}{2(1-v_0^2)}\int_0^z P(\tau,t)d\tau - \frac{P_2(t)}{2(1-v_0^2)}z \tag{29}$$

We know that the influence of the stress tensor components $t_{rz}$ and $t_{rr}$ in the fluid have been incorporated in solving for the components of the membrane displacement. Hence, the genesis of the

aneurysm is in the weakening of the membrane at $r = a_0$. Therefore, (28) and (29) constitute the components that measure the dynamical changes of the aneurysm wall and the deformed radius given in (25) in dimensionless representation, measures the size of the aneurysm radially and whose change with respect to *P(z,t)* may not be linear.

The dimensional equivalent of the aneurysm size is given in (13). The velocity and membrane components and the aneurysm size are completely determined if the pressure functions $P(z,t), P_1(t)$ and $P_2(t)$ are found. For the pressures $P_1(t)$ at the beginning of the aneurysm region $z = 0$ and $P_2(t)$ at the end of the aneurysm region $z = L$, we will use the Milnor [3, 31, 32] pressure waveform

$$P(t) = P_m + \sum_{n=1}^{N}(A_n\cos(n\omega t) + B_n\sin(n\omega t)),$$

where $P_m$ is the mean blood pressure, $A_n$ and $B_n$ are Fourier coefficients for $N$ harmonics, and $\omega$ is the circular frequency. In the case of Brachial Artery aneurysms, $P_1(t)$ and $P_2(t)$ can be taken as the Brachial Artery Peripheral Pulse Pressures measured non-invasively with any of the modern conventional sphygmomanometry. $P_1(t)$ is the diastolic pressure wave form for $N < 10$, and $P_2(t)$ is the systolic pressure waveform for $N \geq 10$.

So, $P = P(z,t)$ is the intra-aneurysmal pressure and from (15), (16), (19), (20) and (26) - (28) it satisfies the nonlinear partial differential equation

$$\frac{1}{16}\left\{1 + \varepsilon\left[\frac{2-v_0}{2(1-v_0^2)}P(z,t) + \frac{v_0}{2(1-v_0^2)}P_2(t)\right]\right\}^3 \frac{\partial^2 P(z,t)}{\partial z^2}$$
$$+ \frac{\varepsilon(2-v_0)}{8(1-v_0^2)}\left\{1 + \varepsilon\left[\frac{2-v_0}{2(1-v_0^2)}P(z,t) + \frac{v_0}{2(1-v_0^2)}P_2(t)\right]\right\}^2\left(\frac{\partial P(z,t)}{\partial z}\right)^2$$
$$- \frac{\varepsilon}{2}\left\{1 + \varepsilon\left[\frac{2-v_0}{2(1-v_0^2)}P(z,t) + \frac{v_0}{2(1-v_0^2)}P_2(t)\right]\frac{1-2v_0}{2(1-v_0^2)} + \frac{2-v_0}{(1-v_0^2)}\right\}\frac{\partial P(z,t))}{\partial t}$$
$$= -\frac{\varepsilon}{4(1-v_0^2)}\left\{1 + \varepsilon\left[\frac{2-v_0}{2(1-v_0^2)}P(z,t) + \frac{v_0}{2(1-v_0^2)}P_2(t)\right] - 2v_0\right\}P_2'(t)$$
$$+ \delta(P(z,t) - P_e) \tag{30}$$

We shall employ the perturbation method of [1, 33] by developing the pressure function $P(z,t)$ in a power series with respect to the small parameter $\varepsilon$ and neglecting the $O(\varepsilon^2)$ terms. That is, we assume that

$$P(z,t) = \sum_{n=0}^{\infty}\frac{\varepsilon^n P_n(z,t)}{n!} \tag{31}$$

Consequently, we have the following system of partial differential equations in $P_0(z,t)$ and $P_1(z,t)$:

$$\frac{1}{16}\frac{\partial^2 P_0(z,t)}{\partial z^2} = \delta[P_0(z,t) - P_e] \tag{32}$$

$$\frac{1}{16}\frac{\partial^2 P_1(z,t)}{\partial z^2} - \delta P_1(z,t) = -\frac{1}{16}\left[3\frac{2-v_0}{2(1-v_0^2)}P_0(z,t) + \frac{3v_0 P_2(t)}{2(1-v_0^2)}\right]\frac{\partial^2 P_0(z,t)}{\partial z^2}$$
$$-\frac{(2-v_0)}{8(1-v_0^2)}\left(\frac{\partial P_0(z,t)}{\partial z}\right)^2 + \frac{1}{4}\left[\frac{1-2v_0}{1-v_0^2}\frac{\partial P_0(z,t)}{\partial t} - \frac{P_2'(t)}{1-v_0^2}\right]$$
$$+\frac{2-v_0}{2(1-v_0^2)}\frac{\partial P_0(z,t)}{\partial t} + \frac{v_0 P_2'(t)}{2(1-v_0^2)} \tag{33}$$

The solution of equations (32) - (33) are solved by direct integration, using the boundary conditions in (24). The perturbation solution is then $P(z,t) = P_0(z,t) + \varepsilon P_1(z,t)$. The expressions for $P_0(z,t)$ and $P_1(z,t)$ are given in Appendix A. The approximate aneurysm wall development using (25) and (28) is given by the equation

$$a(z,t) = 1 + \varepsilon\left[\frac{2-v_0}{2(1-v_0^2)}P(z,t) + \frac{v_0 P_2(t)}{2(1-v_0^2)}\right] \tag{34}$$

Thus, the evolution and development of the aneurysm size is dependent on the following impact forces and parameters: (i) The Poisson ratio, $v_0$, which we henceforth defined as the ratio of the lateral or transversal contraction to longitudinal extension, (ii) The pressures at the beginning of the aneurysm region $z = 0; P_1(t)$ and at the end of the aneurysm region $z = 1, P_2(t)$; The intra-aneurysmal pressure $P(z,t)$, which in turn depends on $v_0$, $P_1(t)$, $P_2(t)$, the rates $P_1'(t)$ of $P_1(t)$ and $P_2'(t)$ of $P_2(t)$ and the filtration velocity coefficient $\delta$. The filtration velocity coefficient $\delta$ accounts for the thinning of the aneurysm wall and contributes to the way the intra-aneurysmal pressure, $P(z,t)$, is moderated. It also accounts for the remodeling and growth of the membrane in response to the tension exerted on it by the forces of fluid flow and stress tensors.

We will now examine the morphology of the aneurysm curvature by establishing conditions determining the extent to which the deformed radius $a(z,t)$ can stretch. As seen in (34), $a(z,t)$ depends on $P(z,t)$ and so the extrema of $a(z,t)$ occurs at the same location within the aneurysm region as those of $P(z,t)$. That is, the morphology of the aneurysmal wall curves the same way in all directions; downward if

$P_{zz} < 0$ or upward if $P_{zz} > 0$ and the morphology can also be up in some direction and down in others. We shall examine these characteristics with respect to the values of the Poisson ratio $v_0$. Theorem 2.1 establishes conditions that allow for a minimum and maximum stretch of the deformed radius and hence aneurysmal curvature. Theorem 2.2 establishes conditions on the Poisson ratio conditioned for aneurysm rupture.

THEOREM 2.1. Let $P$ be twice differentiable with respect to $z$ and $t$ and $\frac{\partial^2 P(z,t)}{\partial z \partial t} = \frac{\partial^2 P(z,t)}{\partial t \partial z}$ such that

$$\frac{\partial^2 P(z,t)}{\partial z^2} \cdot \frac{\partial^2 P(z,t)}{\partial t^2} + \frac{v_0}{2-v_0}\frac{\partial^2 P(z,t)}{\partial z^2}P_2''(t) > \left(\frac{\partial^2 P(z,t)}{\partial z \partial t}\right)^2,$$

and $v_0 \in [0,1) \cup (1,2) \cup (2,\infty)$. If $a(z,t)$ given in (34) is twice differentiable in $z$ and $t$ then the aneurysm wall attains a minimum extension at some point $z \in (0,1)$ for all $t \geq 0$ provided

$$\varepsilon f(v_0, P(z,t), P_2)P_2''(t) + g(v_0)(P(z,t) - P_e) > 0$$

Similarly, if

$$\varepsilon f(v_0, P(z,t), P_2)P_2''(t) + g(v_0)(P(z,t) - P_e) < 0$$

then the aneurysm wall attains a maximum extension where

$$f(v_0, P(z,t), P_2) = \frac{1}{(1-v_0^2)(2-v_0)}\left\{\frac{2-v_0}{2(1-v_0^2)}P(z,t) + \frac{v_0}{2(1-v_0^2)}P_2(t)\right\}$$

and

$$g(v_0) = \frac{2\delta}{v_0^2 - v_0 + 1}$$

Furthermore, the aneurysm curvature is up in one direction and down in the other if

$$\frac{\partial^2 P(z,t)}{\partial z^2} \cdot \frac{\partial^2 P(z,t)}{\partial t^2} + \frac{v_0}{2-v_0}\frac{\partial^2 P(z,t)}{\partial z^2}P_2''(t) < \left(\frac{\partial^2 P(z,t)}{\partial z \partial t}\right)^2$$

*Proof.* *a(z,t)* is differentiable in *z* and *t* since *P(z,t)* is and from equation (34), we see that the equilibrium points occurs when $\frac{\partial P}{\partial z} = 0$ and $\frac{\partial P}{\partial t} = -\frac{v_0}{2-v_0}P_2'(t); v_0 \neq 2$. Upon substituting the equilibrium points into the pressure equation in (30) we

see that $\dfrac{\partial^2 P}{\partial z^2} > 0$ for a minimum extension and $\dfrac{\partial^2 P}{\partial z^2} < 0$

for a maximum extension and $\dfrac{\partial^2 a}{\partial z^2} \cdot \dfrac{\partial^2 a}{\partial t^2} - \left(\dfrac{\partial^2 a}{\partial z \partial t}\right)^2 > 0$ .

Furthermore, $\dfrac{\partial^2 P}{\partial z^2} \cdot \dfrac{\partial^2 P}{\partial t^2} + \dfrac{v_0}{2 - v_0} \dfrac{\partial^2 P}{\partial z^2} P_2''(t) < \left(\dfrac{\partial^2 P}{\partial z \partial t}\right)^2$ ,

gives that $\dfrac{\partial^2 a}{\partial z^2} \cdot \dfrac{\partial^2 a}{\partial t^2} - \left(\dfrac{\partial^2 a}{\partial z \partial t}\right)^2 < 0$ and the theorem holds.

THEOREM 2.2. Let $a(z,t,v_0)$ be given in (34) and $P(z,t) = P_0(z,t) + \varepsilon P_1(z,t)$ . Then, there exists a functional $M(z,t,v_0, P_1(t), P_1'(t), P_2(t), P_2'(t))$ such that for $z_0$ and $t_0$ fixed, we have

$$\left|(1-v_0)^2 a(z_0,t_0,v_0)\right| \leq \frac{1}{4}\left|M(z_0,t_0,v_0,P_1(t_0),P_1'(t_0),P_2(t_0),P_2'(t_0))\right|$$
and
$$\lim_{v_0 \to 1}\left|(1-v_0)^2 a(z_0,t_0,v_0)\right| \leq N$$

where *N* > 0 is a constant. Furthermore, there exists

$\tilde{N} = \tilde{N}(z,t,v_0, P_1(t), P_1'(t), P_2(t), P_2'(t))$ that is finite and positive at each fixed point $(z_0,t_0)$ given that 0 < *z* < 1 and *t* ≥ 0 such that

$$\lim_{v_0 \to 1}\left|(1-v_0)^2 a(z_0,t_0,v_0)\right| \leq \tilde{N}(z_0,t_0,v_0,P_1(t_0),P_1'(t_0),P_2(t_0),P_2'(t_0)).$$

Similarly, there exists $N_1 = N_1(z,t,v_0, P_1(t), P_1'(t), P_2(t), P_2'(t))$ and

$N_2 = N_2(z,t,v_0, P_1(t), P_1'(t), P_2(t), P_2'(t))$ which are finite and positive at each fixed point $(z_0,t_0)$ such that

$$\lim_{v_0 \to 1}\left|(1-v_0)^2 \xi(z_0,t_0,v_0)\right| \leq N_1 \text{ and}$$
$$\lim_{v_0 \to 1}\left|(1-v_0)^2 \zeta(z_0,t_0,v_0)\right| \leq N_2 \text{ for all points}$$
$(z,t) \in (0,1) \times 0, \infty).$

*Proof.* The proof is a direct consequence of (28), (29), (34) and the perturbation expression for the intra-aneurysmal pressure $P(z,t)$ .

We note that Theorem 2.2 says that $v_0 = 1$ is a singularity of the deformed radius $a(z,t,v_0)$ and the components of the membrane displacement $\xi(z,t,v_0)$

and $\zeta(z,t,v_0)$ . Consequently, they blow up as $v_0$ approaches one. This implies that the aneurysm may rupture at some point $z_0; 0 < z_0 < 1$ and time $t \geq t_0$ for some fixed $t_0$ . However, for $v_0 \neq 1$ , the transversal and longitudinal components of the membrane displacement remain bounded for fixed $(z_0,t_0)$ . Consequently, the aneurysm wall remains stable at any fixed point $(z_0,t_0); 0 \leq z_0 \leq 1; t \geq t_0$ , when $v_0 \neq 1$ .

## 2.1. The Impact of Filtration and Fluid Flux

In this section, we examine the impact of filtration and the total fluid flux on the aneurysm wall. In dimensionless parameters, the filtration velocity $v_{n,f}$ is given as

$$v_{n,f} = \delta(P(z,t) - P_e) \tag{35}$$

which is completely defined by the perturbation solution for $P(z,t)$ . The total flux crossing the undeformed radius, denoted by $Q_{n,f}$ , is given as

$$Q_{n,f} = \iint_{\Sigma} v_{n,f} d\sigma \tag{36}$$

where $d\sigma = a(z,t)\sqrt{1 + \left(\dfrac{\partial a}{\partial z}\right)^2} d\theta dz; 0 \leq \theta \leq 2\pi; 0 \leq z \leq L$ ,

and $\Sigma$ is the whole surface of the aneurysm region. In dimensionless parameters, $Q_{n,f}$ is given as

$$Q_{n,f} = \delta \int_0^1 a(z,t)[P(z,t) - P_e] dz.$$

The profile of the impact of the filtration flux is given in subsection 3.3, when $O(\varepsilon^2)$ terms of the series solution are neglected. On the other hand, the total fluid flux, $Q(z,t)$ in any cross-section of the aneurysm given in dimensionless parameters is

$$Q(z,t) = 2^\pi \int_0^{a(z,t)} r u(z,r,t) dr \tag{37}$$

which is completely defined by (27), and (34). The profile is given in subsection 3.3.

The filtration velocity as with the pressure, deformed radius and components of the membrane displacement depends on the Poisson ratio $v_0$ . Numerical analysis of the filtration rate shows that the flux blows up as $v_0$ approaches one. A similar conclusion is reached for the case of total fluid flux $Q(z,t)$ .

So for any fixed point $(z_0, t_0); 0 < z_0 < 1; t_0 \geq 0$, if the Poisson ratio approaches one, both $Q_{n,f}$ and $Q(z,t)$ blows up, indicating the potential for rupture.

## 3. NUMERICAL METHODS AND PARAMETERS

Human aneurysms are formed in different sizes and shapes, and they exhibit a variety of material behavior [6, 8, 10, 13]. As indicated earlier much of the work geared towards understanding the development and evolution of an aneurysm has focused mostly on the fluid content dynamics, shape and size. The current interests are to determine more reliable parameters to predict the potential for aneurysmal rupture. So, we will use the data collected in the literature [6, 8-10, 13, 31, 34] to fit the mathematical model developed in section 2. We have considered an aneurysm within a cylindrical portion of a blood vessel of length $L = 2cm$, a membrane of thickness $h = 0.25cm$, and an undeformed radius of $a_0 = 0.5cm$. We also considered a permeability coefficient of $k^* = 2.5 \times 10^{-7}$ and the Darcy-Starling coefficient $\delta = \dfrac{k^* L^2}{h a_0^3}$. For the end pressure $P_1(t)$ and $P_2(t)$, we shall considered the Ferguson [3, 6, 31] pressure formula described by the Fourier series

$$P_i(t) = P_m + \sum_{n=1}^{N} [A_n \cos(n\omega t) + B_n \sin(n\omega t)]; i = 1, 2.$$

Milnor [3, 6, 31, 32] suggested that $N = 10$ is sufficient to describe systemic blood pressure in general with $N < 10$ in the diastole vasculature. Here, we shall take $P_1(t)$ to represent the diastolic pressures and $P_2(t)$ the systolic pressures. All pressure measurements considered here are in $mmHg$. We shall take $P_m = 65.7 mmHg$, see [6], the coefficients of the Fourier series given in row vector form are:

$$A_n = [-7.13 \quad -3.08 \quad -0.130 \quad -0.346 \quad 0.0662 \quad \ldots]$$

$$B_n = [4.64 \quad -1.18 \quad -0.564 \quad -0.346 \quad -0.120 \quad \ldots]$$

and we have taken $P_e = 70 mmHg$ where we have used the Shah and Humphrey data in [6].

Since the heart beats about 72 times per minute, we shall take $\dfrac{2\pi}{\omega} = \dfrac{60}{72}$, or $\omega = 8 rad/s$ for a regular heart beat. As deduced in section 2, the mathematical model developed is a quasi-static form of a slow flow. Consequently in dimensionless parameters, the fluid characteristics such as density and viscosity do not

figure in the numerical solutions. The surviving parameters are size of the aneurysm region, $L$, permeability and filtration coefficient $\delta$, undeformed radius $a_0$, membrane thickness, $h$, the Poisson ratio $v_0$, and the time scale. All of which can be measured by noninvasive means. Intra-aneurysmal pressure $P(z,t)$, fluid flow patterns, membrane displacement and the dynamics of the deformed radius are expressed in terms of the surviving parameters. As can be seen, the numerical results given here indicate that the Poisson ratio, intra-aneurysmal pressure gradients, flow profiles and membrane displacement could provide additional information regarding the rupture potential of aneurysms.

Towards that end, we use the MATLAB® platform version 7.10, 207B, 208B to numerically and graphically understand the roles the bloodstream impact forces, intra-aneurysmal pressure elevations and Poisson ratio play in the rupture potential of aneurysms contained within cylindrical portions of blood vessels. The method begins with the dimensionless solutions of the fluid velocity components $v(z,r,t)$, $u(z,r,t)$; the membrane displacement components $\xi(z,t)$, $\zeta(z,t)$; the deformed radius $a(z,t)$; the intra-aneurysmal pressure, $P(z,t)$; the filtration velocity, $v_{nf}$; the rate of filtration $Q_{nf}$, and the cross-sectional fluid flux $Q(z,t)$. We have developed MATLAB® codes of these solutions to produce numerical data and graphical representation at the circular frequencies $\omega = 2\pi f$ where $f = 0.2, 0.5, 1, 1.2, 5, 8, 10$ to simulate *in vitro* tests. It is known that most actual laboratory tests are performed at values of $f$ at 0.1 or 0.2 [6, 31]. The impact of the Poisson ratio on the comparative relationship of the deformed radius, $a(z,t)$, with intra-aneurysmal pressure, $P(z,t)$, and with the local elevations of the intra-aneurysmal pressure is expressed for the Poisson ratio ranges of $0 < v_0 < 1, 1 < v_0 \leq 2$, and $v_0 > 2$.

### 3.1. Results and Analysis

Computations revealed discontinuity in the profiles of the impact fluid velocity and its components, the membrane displacement and its components, the intra-aneurysmal pressure, the deformed radius, the rate of filtration and the flux on any cross-section of the membrane within the aneurysm region when the Poisson ratio approaches 1. We shall interpret the points of discontinuity in the solution profiles as indicators for aneurysm rupture. The dynamic profiles of the bloodstream impacting forces, intra-aneurysmal pressure elevations and the deformed radius exhibit similar characteristics for $f = 0.1, 0.2, 0.5, 1, 1.2,$ and 5.

However, we shall present the results for the cases $f = 1.2$ corresponding to the regular heart beat of 72 beats per minute, and $f = 0.2$, the experimental value at irregular heart beat of 12 beats per minute. In each case, we considered two scenarios, the case where a fixed point $(z_0, t_0)$ is considered within the aneurysm and one where all points $(z, t)$ are considered within the aneurysm region. In both cases, we see that for $f = 0.2$ and $f = 1.2$, time changes of the simulations of the intra-aneurysmal pressure, $P(z, t)$ are in synchrony with the membrane displacement components, its magnitude and the deformed radius (See Figures **2, 3, 12, 13** and **13**). For the figures presented here, we maintained $P_1(t)$ and $P_2(t)$ at the same oscillating values. Even when one end is maintained at higher pulsating pressure values there were no significant differences, in regards to rupture potential indicators, in the characteristics of the profiles of the intra-aneurysmal pressure, membrane displacement, deformed radius, filtration velocity, filtration rate and fluid flux.

In Figures **2** and **3**, the profile of the deformed radius $a(z, t)$ is flat before and after the discontinuity. However, in Figure **10** which is associated with the case of a regular heart beat, it shows local elevations before the discontinuity at the time $v_0 = 1$ and then it oscillates with time afterwards to vanish. In Figure **11** corresponding to the case of irregular heart beat, the profile of the deformed radius increases before the

discontinuity and then drops gradually after the discontinuity and then oscillates and die out. In Figures **10** and **11**, the intra-aneurysmal pressure, $P(z, t)$ shows local pressure elevations before the discontinuity. Following the point of discontinuity, the pressure profile drops and then elevates and then oscillates and die out. The transversal component of the membrane displacement shows the same characteristics with the deformed radius, $a(z, t)$. But this is not surprising, since $a(z, t) = 1 + \varepsilon \xi(z, t)$. The longitudinal component of the membrane displacement elevates slightly followed by a drop leading into the point of discontinuity, then delays afterwards slightly and elevates, then oscillates to vanish. The profiles of the impact fluid velocity in Figure **10** and **11** shows elevated values leading into the point of discontinuity and oscillates to zero afterward. Similarly, the profile of the magnitude of the membrane displacement elevates rapidly leading to the point of discontinuity and then oscillates to zero afterward. There are more oscillations following the point of discontinuity for the case of a regular heart beat than the case of irregular heart beat.

### 3.2. Impact of the Poisson Ratio on the Relationship of $a(z, t)$ with $P(z, t)$

The impact of the Poisson ratio on the relationship between the deformed radius and intra-aneurysmal pressure can be seen from the linear relationship between $a(z, t)$ and $P(z, t)$ given in equation (34) for values of $v_0 \in (0, 1)$.
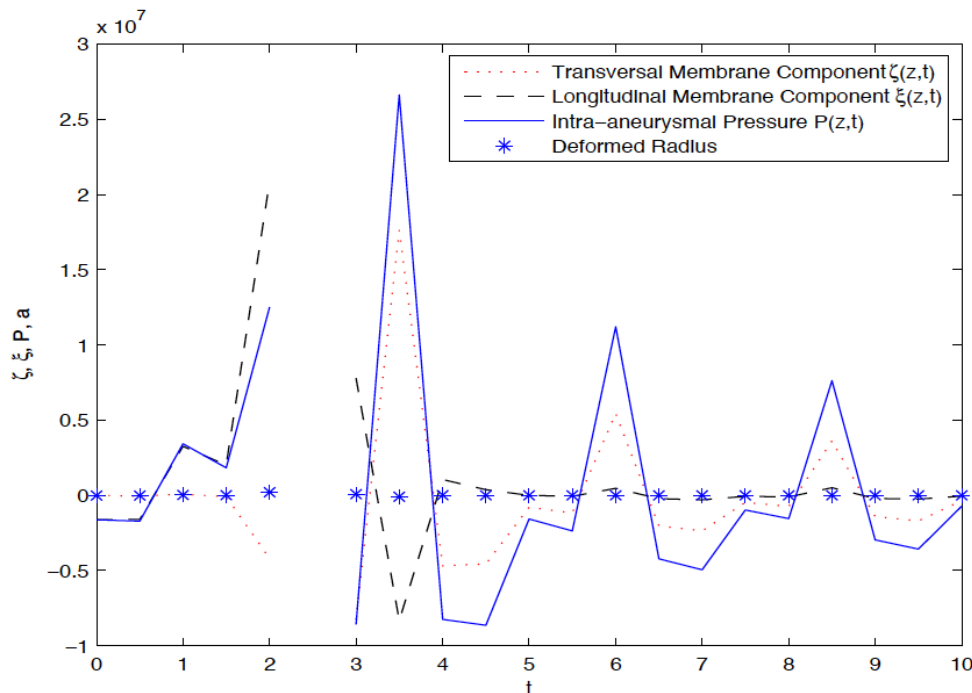


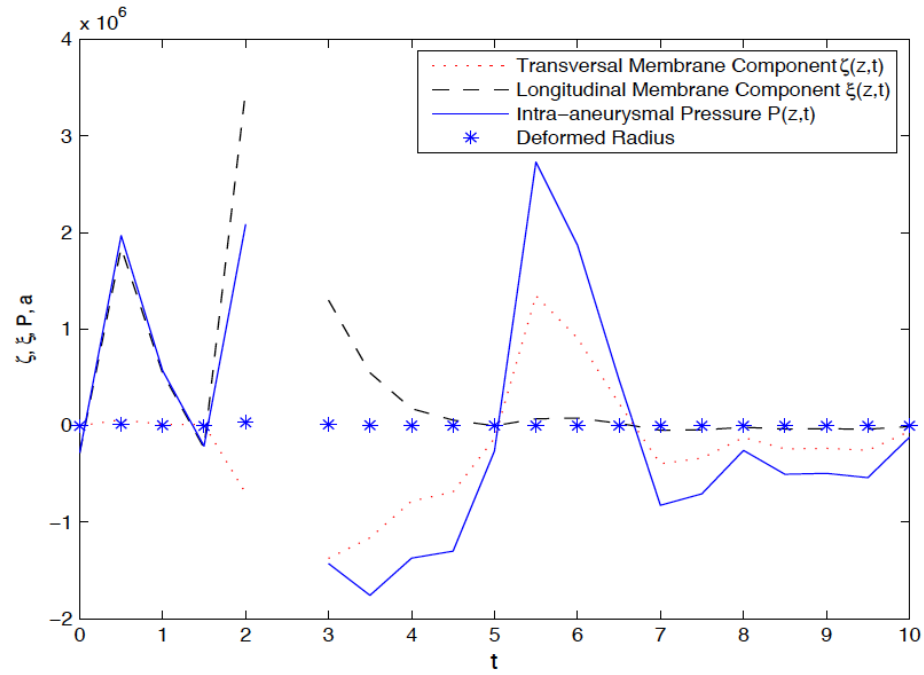**Figure 2:** Membrane displacement, deformed radius, pressure vs time, *f* = 1.2 , *z* and $v_0$ varies.

**Figure 3:** Membrane displacement, deformed radius, pressure vs time, *f* = 0.2, *z* and $v_0$ varies.
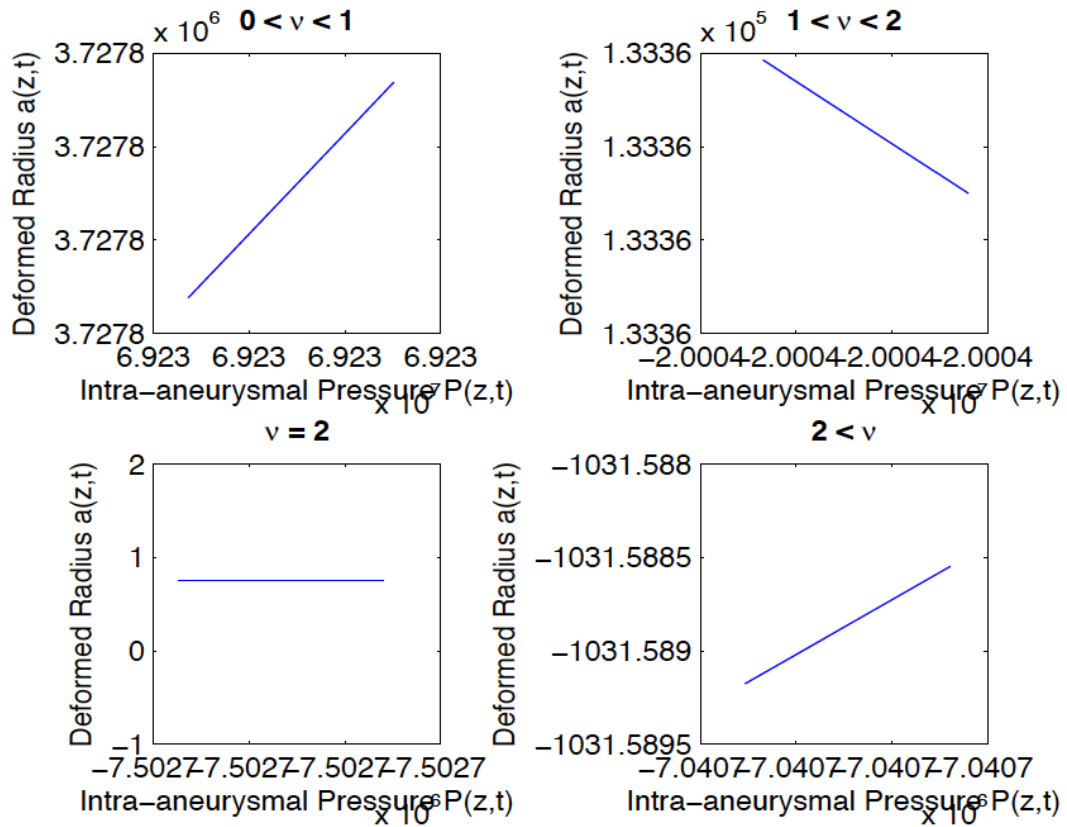


**Figure 4:** *a(z,t)* vs. *P(z,t)* for fixed *z*.

We see from Figure **4** that at a fixed point $(z_0, t_0)$ within the aneurysm, $a(z,t)$ increases linearly with $P(z,t)$ before the point of discontinuity. For values of $v_0 \in (1,2)$ after discontinuity, $a(z,t)$ decreases linearly with increasing $P(z,t)$. When $v_0 = 2$, $a(z,t)$ remains

constant at the point $(z_0, t_0)$, since $P_2(t_0)$ is constant. For $v_0 > 2, a(z,t)$ again increases with $P(z,t)$.

When $(z,t)$ varies within the aneurysm region, we see in Figure **5** that the relationship for $0 < v_0 < 1, 1 < v_0 < 2$ and $v_0 > 2$ is not linear. The curvature display concavity. Thus, by Theorem 2.1 of section 2, the aneurysm curvature attains maximal or minimal stretches and exhibit saddle point behavior.

In Figures **2** and **3**, we see that the intra-aneurysmal pressure is in synchrony with the longitudinal component of the membrane displacement before the discontinuity with elevated values leading to the point of discontinuity. After the discontinuity, the pressure and the transversal component of the membrane displacement are in synchrony, delaying right after the discontinuity and then peaking and then pulsating to vanish. We note that the oscillations are more rapid in the case of the regular heart beat in Figure **2** than the case of irregular heart beat in Figure **3**. In Figures **6** and **7** we considered the usual experimental Poisson ratio value of $v_0 = 0.45$. Results shows the profiles of the impacting forces and membrane displacement with respect to time as seen in most of the literature [5, 6]. There are no breaks in the graphs and they exhibit pulsating characteristics at the irregular heart beats

and regular heart beats frequencies $f = 0.2$ and $f = 1.2$ respectively. The same observations are seen when $v_0 = 1.2$ in Figures **8** and **9**. Similarly, we see in Figures **12** and **13**, the profiles of the magnitude of the membrane displacement and the intra-aneurysmal pressure are in synchrony for $v_0 = 0.45$ and $v_0 = 1.2$ with respect to time. In Figure **14**, we display the profiles of the relationship between the transversal and longitudinal membrane displacements, intra-aneurysmal pressure and the deformed radius with respect to time when $v_0 = 1.2$. A similar profile is observed for $v_0 = 0.45$.

### 3.3. The Role of Filtration and Membrane Thickness

In Figure **15**, we present the time varying profiles of the filtration velocity, filtration rate, and the fluid flux. The graphs have a discontinuity at the time of aneurysm rupture. In Figure **16**, we presented the thickness varying relationship to the filtration velocity and rate and the deformed radius at the regular heart beat and in Figure **17** at the irregular heart beat. We observed that the graphs exhibited a discontinuity at the membrane thickness of about 0.05cm from 0.25cm. That is, the aneurysm may rupture when 80% of the membrane thins out.
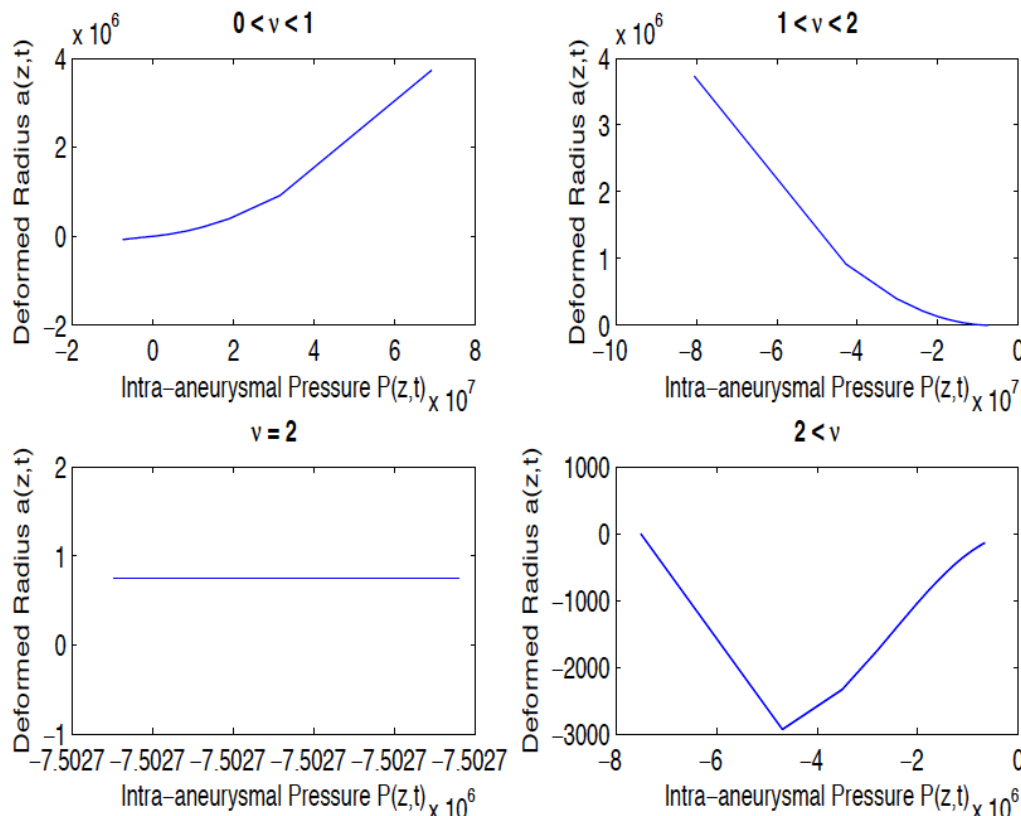


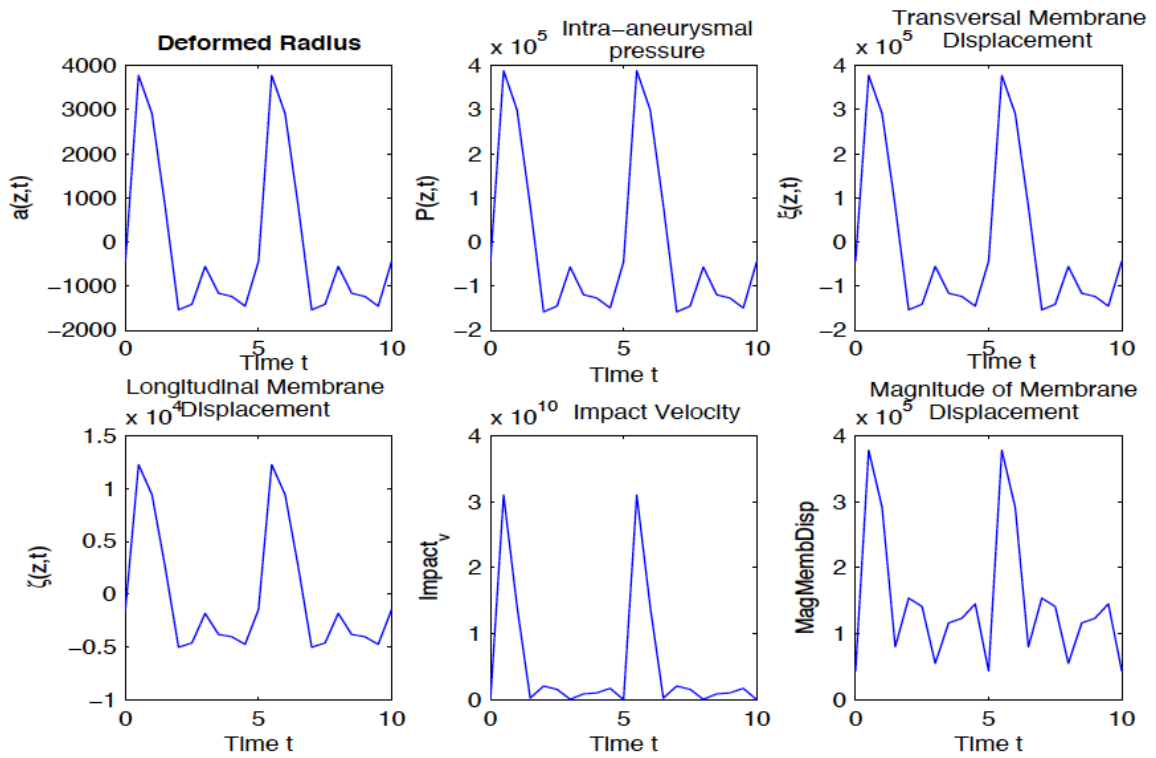**Figure 5:** *a(,z,t)* vs. *P(z,t)* for all *z*.

**Figure 6:** Profile of solutions for $v_0 = 0.45$, $f = 0.2$.
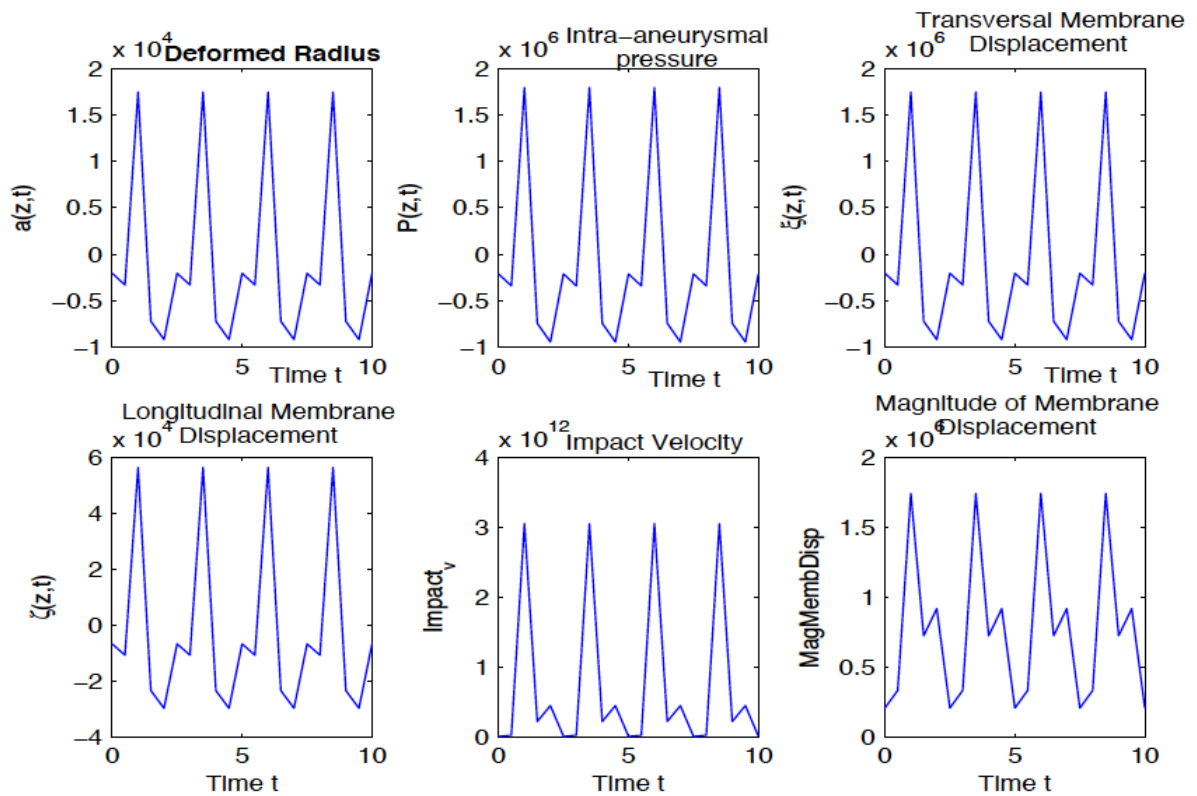
**Figure 7:** Profile of solutions for $v_0 = 0.45$, $f = 1.2$.
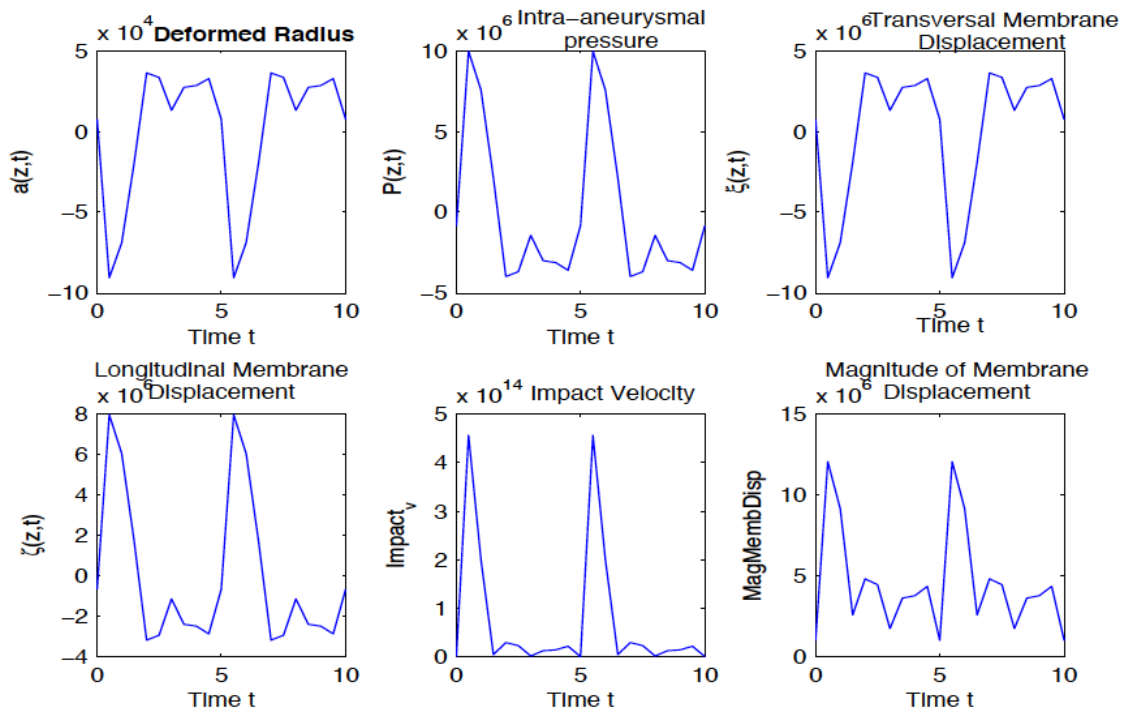
**Figure 8:** Profile of solutions for $v_0 = 1.2$, *f* = 0.2.
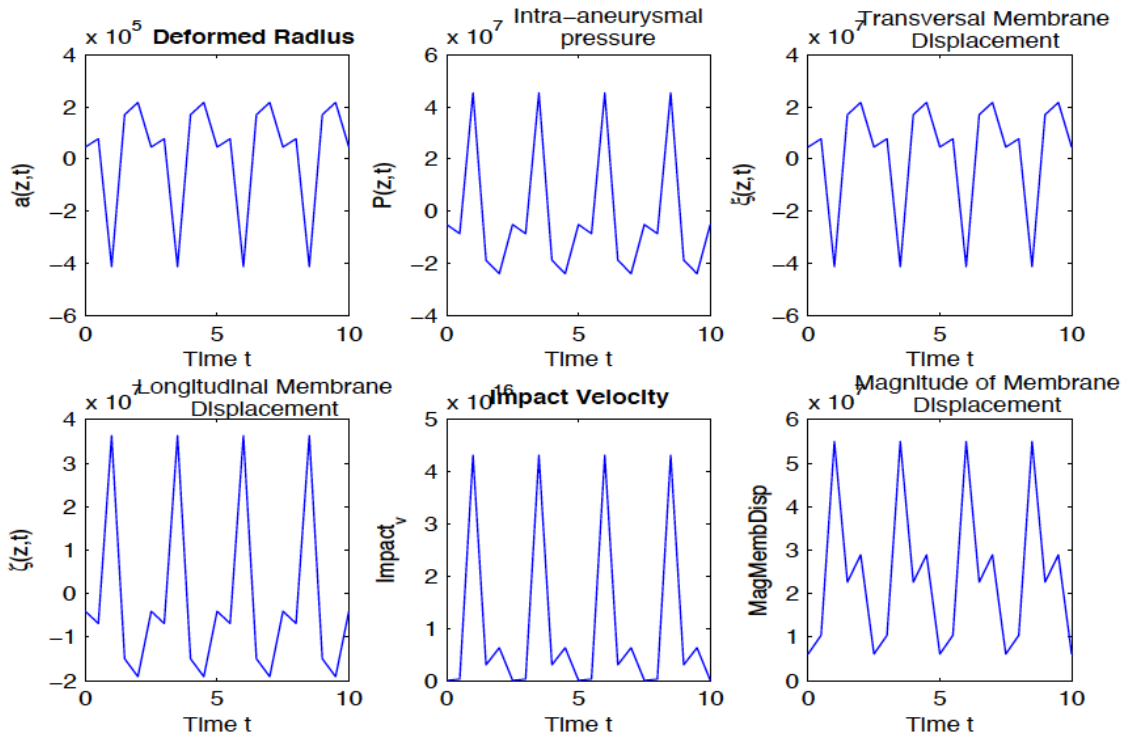


**Figure 9:** Profile of solutions for $v_0 = 1.2$, *f* = 1.2.

## 4. POST RUPTURE ANALYSIS

Aneurysm rupture leads to the development of vasospasm and vasospasm is the leading cause of disability and death from aneurysm rupture [17, 23, 35]. Ruptured aneurysms are most likely to rebleed within the first day with the risk remaining very high for the first two weeks if left untreated [17, 19, 23, 35]. Open
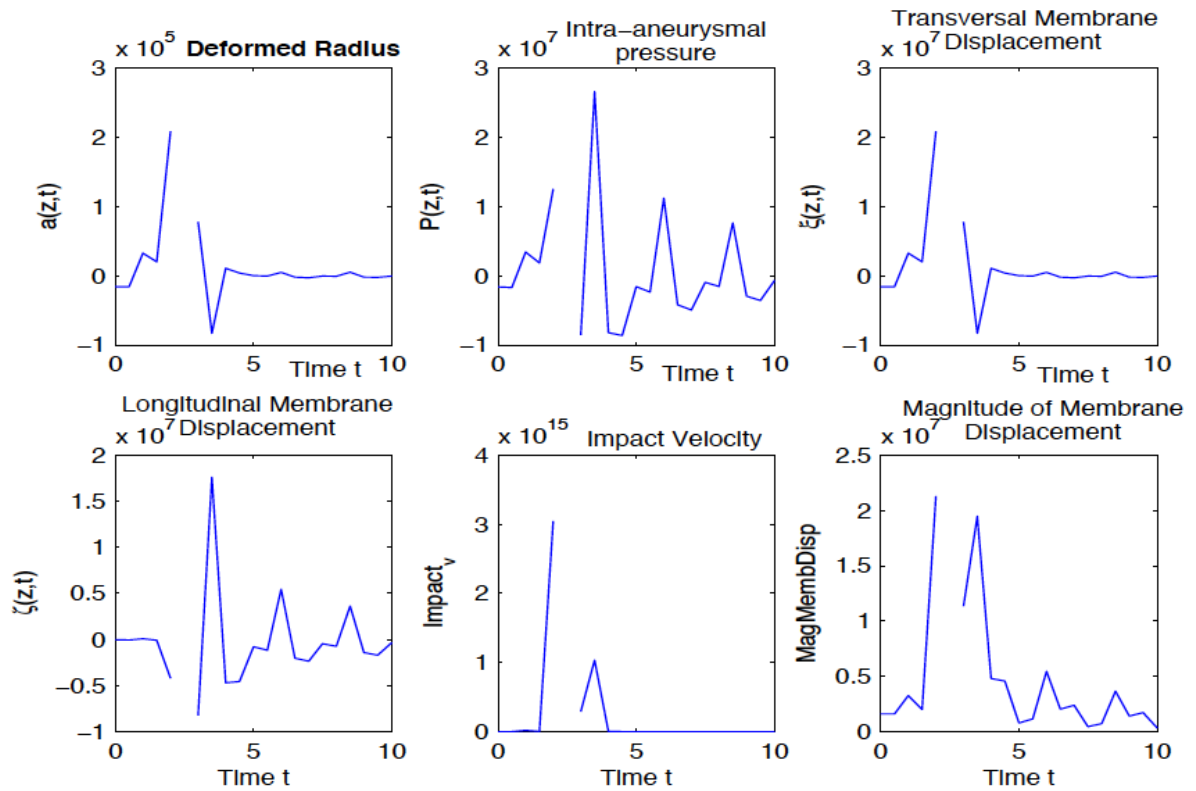
**Figure 10:** Profile of solutions for varying $v_0$, $f = 1.2$.
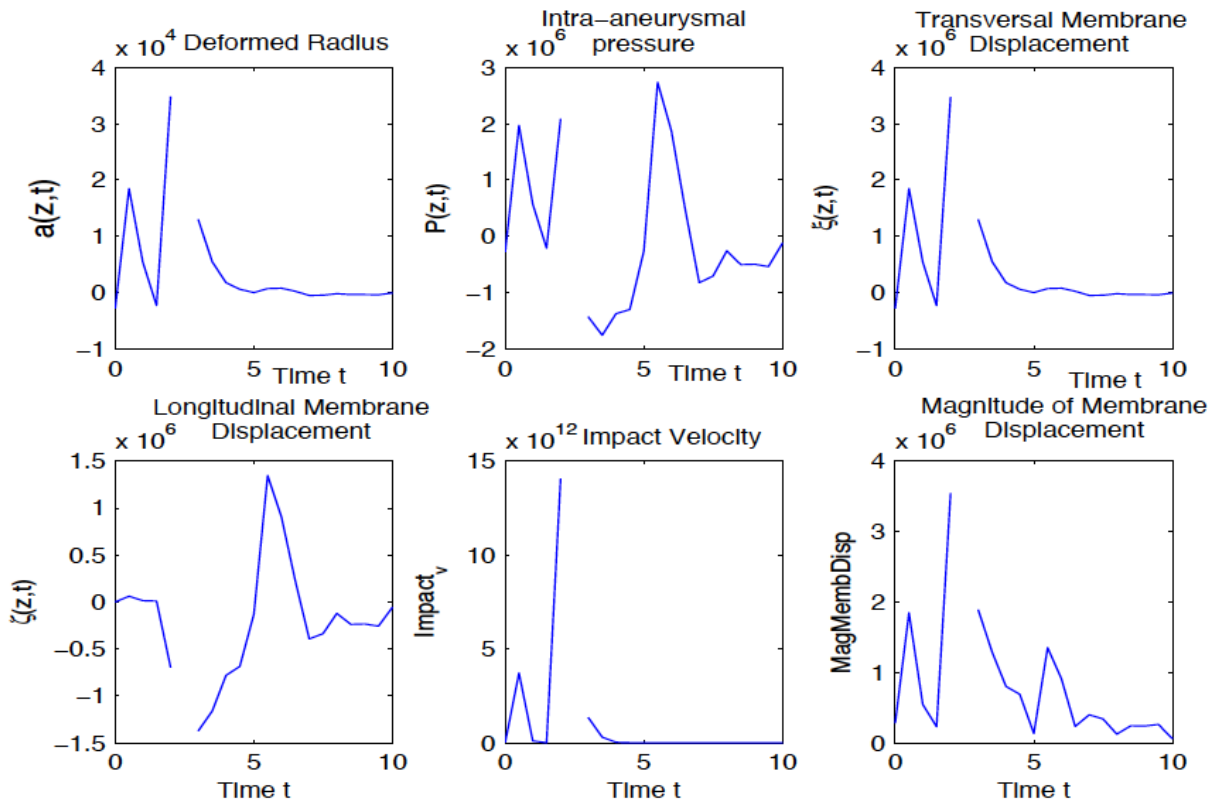


**Figure 11:** Profile of solutions for varying $v_0$, $f = 0.2$.
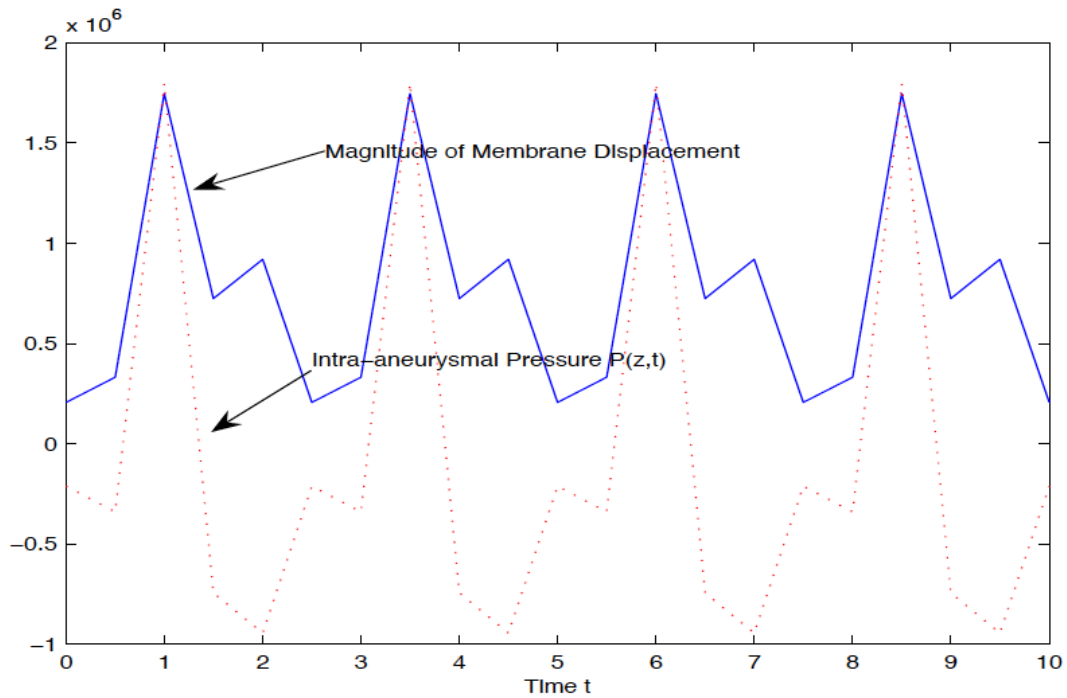
**Figure 12:** Membrane Mag, *P(z,t)* vs time for $v_0 = 0.45$.
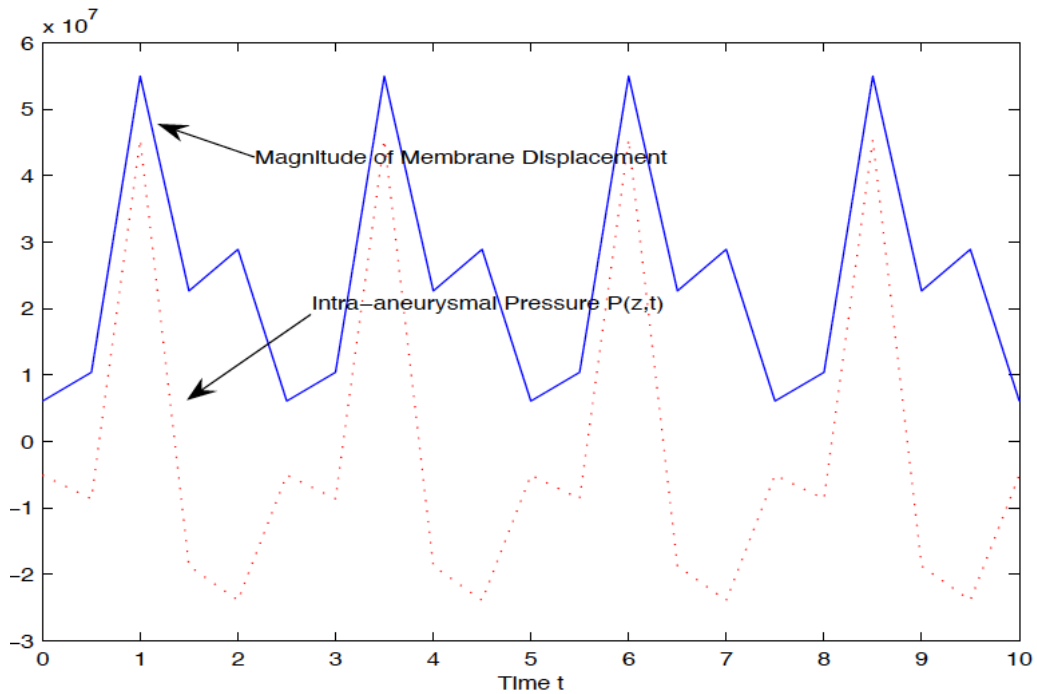


**Figure 13:** Membrane Mag, *P(z,t)* vs time for $v_0 = 1.2$.

surgery and clipping, endovascular coiling and catheter or stent insertion, and aggressive treatment of vasospasm are the most common methods of treatment that have been correlated with improved outcome [17, 23, 36]. The problem is, most aneurysms do not cause symptoms until they rupture. When they rupture, they are associated with significant morbidity and mortality if treatment is not sought on time. Therefore, there is need for a clinical method that measures the levels of severity of aneurysmal subarachnoid hemorrhage and which enables the decision on the best clinical approach for stabilizing the affected portion of the vessel and the method of treatment. Currently, the two widely used methods for
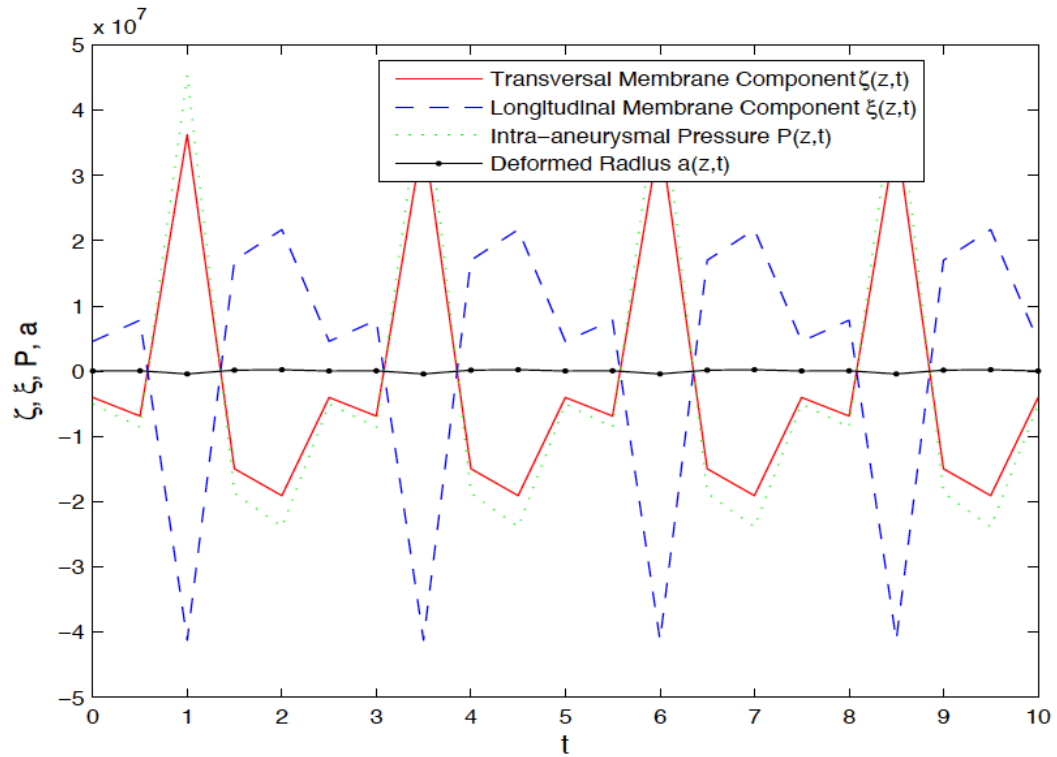
**Figure 14:** Membrane Displacement Components, Pressure, and Deformed Radius vs Time at $v_0 = 1.2$.
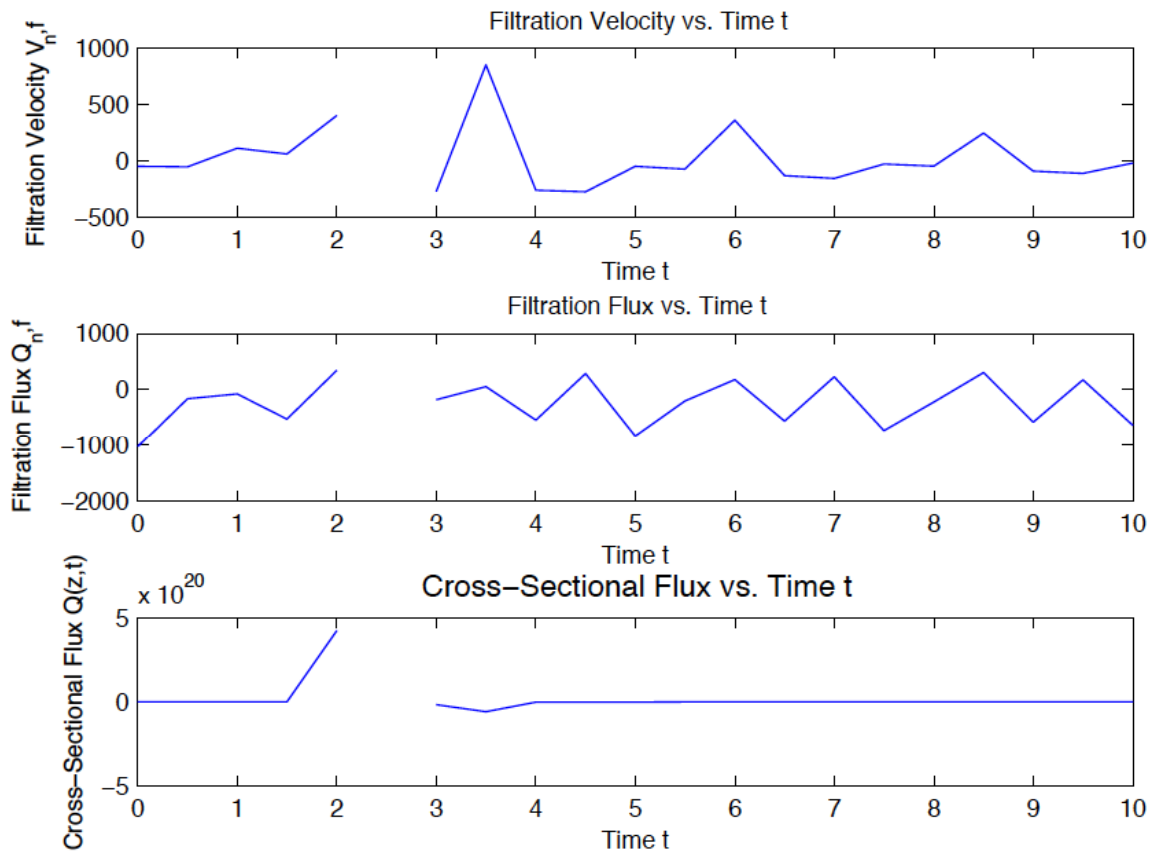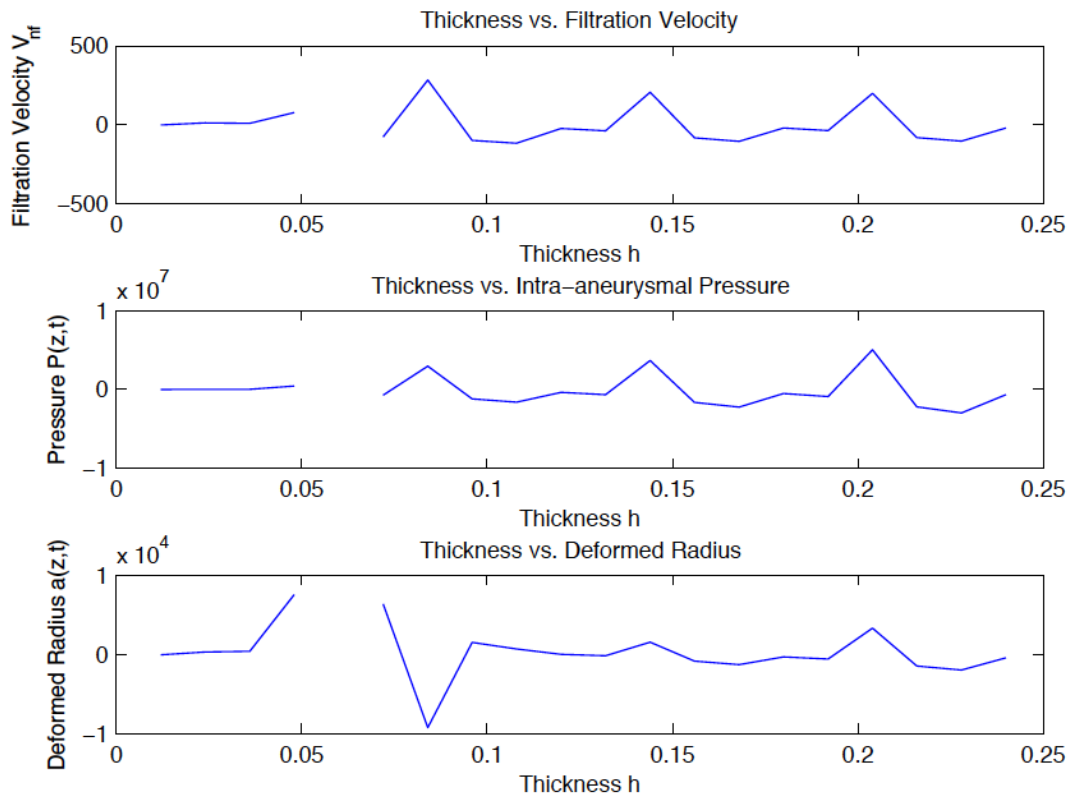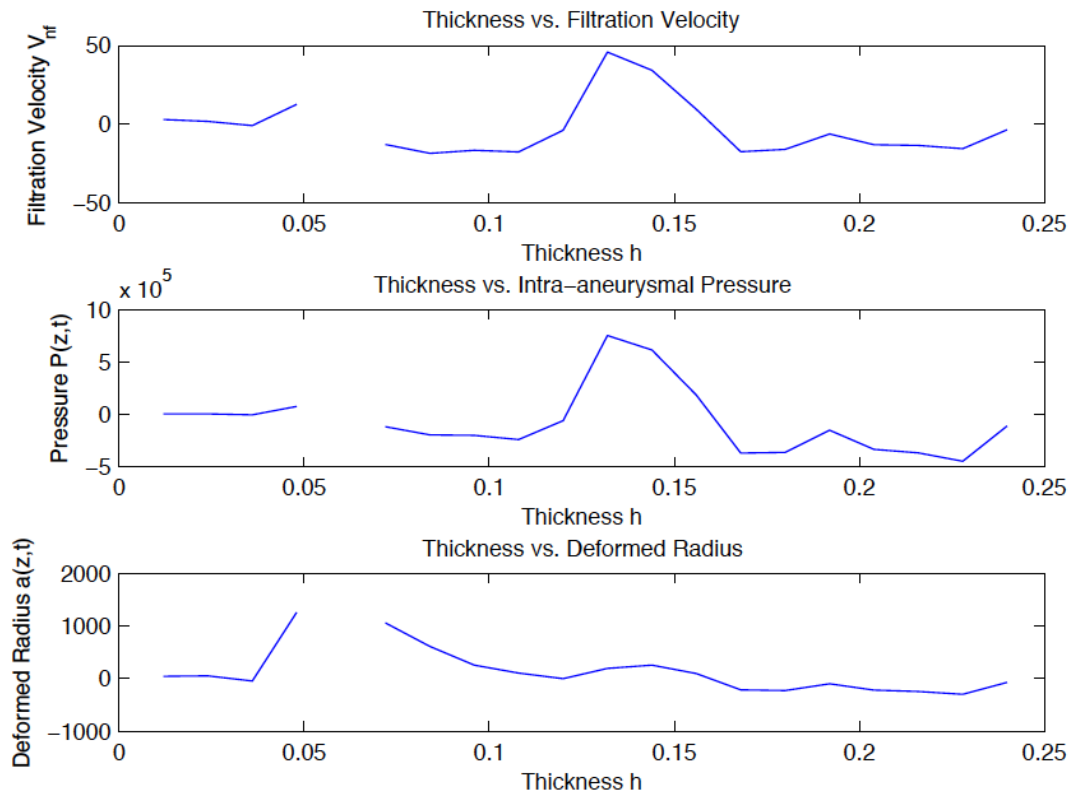


**Figure 15:** Plots of Filtration velocity, Filtration flux, and the Cross-sectional flux vs time.

**Figure 16:** Plots of Intra-aneurysmal pressure, the deformed radius, and filtrationvelocity against the thickness of the wall membrane with varying $v_0$ , *f* = 1.2.



**Figure 17:** Plots of Intra-aneurysmal pressure, the deformed radius, and filtrationvelocity with the thickness of the membrane wall with varying $v_0$ , *f* = 0.2.

grading the clinical severity of ruptured aneurysms are the Hunt and Hess six-point scale and the Fisher 4-point grades [17, 37]. The grade levels for these scales are determined by the level of blood on a CT scan. However, an aneurysm rupture can be severe and the CT scan may have no blood images. For example, the vasospasm is most common in Fisher grade level three which indicate the presence of localized clot or vertical layers less than 1mm thick, but it is rarely found in patients with no blood on CT scans [17, 19, 38, 36].

The profiles of the Intra-aneurysmal pressure $P(z,t)$, the membrane thickness h and the Poisson ratio after an aneurysm rupture given in Figures **2-5, 8-11** and **14-17** can provide a means for an alternative grading scale for measuring the severity of an aneurysm rupture that is not predicated by the presence of blood on a CT scan. The parameters can be used to noninvasively measure the membrane extensional rigidity $D = \dfrac{Eh}{1-v_0^2}$ after an aneurysm has ruptured and therefore, determine the severity of the rupture according to the values of the Poisson ratio extrapolated from the readings of the intra-aneurysmal pressure and membrane thickness. In the range $0 < v_0 < 1$, the extensional rigidity D is positive. It is positive and large for small values of $v_0$, meaning that the membrane wall can be repaired or retracted to its original form [39, 40]. For values of the Poisson ratio in the range $1 < v_0 < 2$, during aneurysm rupture, the membrane extensional rigidity D is negative, meaning that the aneurysm wall is weakened and cannot be retracted to its normal position. With further study, aneurysm rupture severity grading scale range can be developed which incorporate the readings of the Intra-aneurysmal pressure, membrane thickness h, the Poisson ratio, and the membrane extensional rigidity D in deciding which treatment method to use in cases of ruptured aneurysms.

## 5. DISCUSSION

This study reports an analysis of a non-convectional acceleration axi-symmetric blood flow through a cylindrical shaped blood vessel containing an aneurysmal region. The model considers the deformed radius as the appearance of the aneurysm within the blood vessel of length L. In this context, we used the expressions for the deformed radius and membrane displacement to establish the dynamic evolution, development and rupture potential of aneurysms, side wall aneurysms in particular, could be a good fit for the model. We found that the intra-aneurysmal pressure, membrane thickness and the Poisson ratio are parameters that can be used for noninvasive prediction of the risks for aneurysm rupture. We have also seen

that the common dependent forces that influence the dynamics of the impact flow velocity and its components, the membrane displacement and its components, the deformed radius and pressure is the Poisson ratio. The profile of solutions in the post rupture analysis may help to provide insights in developing an aneurysm severity grading scale for deciding the best treatment and management of ruptured aneurysms. The numerical results are computed within the inbuilt allowable approximations of MATLAB® and hence are amenable to improvement through other computational techniques and larger data values.

We hope that the results presented here will bring further insights in developing noninvasive means for detecting the potential of an aneurysm to rupture and even the ability to develop preventive procedures based on patient symptoms.

## ACKNOWLEDGEMENT

## APPENDIX: THE STANDARD EXPRESSIONS FOR $P_0(z,t)$ AND $P_1(z,t)$

$$P_0(z,t) = \alpha(t)e^{4\sqrt{\delta z}} + \beta(t)3^{-4\sqrt{\delta z}} + P_e$$

$$P_1(z,t) = \gamma(t)e^{4\sqrt{\delta z}} + \lambda(t)3^{-4\sqrt{\delta z}} + \frac{1}{8\sqrt{\delta}}g_1(t)ze^{4\sqrt{\delta z}}$$

$$-\frac{1}{8\sqrt{\delta}}g_2(t)ze^{-4\sqrt{\delta z}} + \frac{1}{48\delta}g_3(t)e^{8\sqrt{\delta z}} \qquad (38)$$

$$+\frac{1}{48\sqrt{\delta}}g_4 e^{-8\sqrt{\delta z}} - \frac{g_5(t)}{16\delta}$$

where

$$\alpha(t) = \frac{P_2(t) - P_1(t)e^{-4\sqrt{\delta}} - P_e(1 - e^{-4\sqrt{\delta}})}{2\sin h(4\sqrt{\delta})}$$

$$\beta(t) = \frac{P_2(t) - P_1(t)e^{4\sqrt{\delta}} - P_e(1 - e^{4\sqrt{\delta}})}{2\sin h(4\sqrt{\delta})}$$

$$g_1(t) = \frac{4}{1-v_0^2}\{(5-4v_0)\alpha'(t) - 6\delta[(2-v_0)P_e + v_0 P_2(t)]\alpha(t)\}$$

$$g_2(t) = \frac{4}{1-v_0^2}\{(5-4v_0)\beta'(t) - 6\delta[(2-v_0)P_e + v_0 P_2(t)]\beta(t)\}$$

$$g_3(t) = -\frac{56(2-v_0)}{1-v_0^2}\delta\alpha^2(t)$$

$$g_4(t) = -\frac{56(2-v_0)}{1-v_0^2}\delta\beta^2(t)$$

$$g_5(t) = \frac{4}{1-v_0^2}[(2v_0-1)P_2'(t) + 4\delta(2-v_0)\alpha(t)\beta(t)]$$

$$\gamma(t) = \frac{1}{2\sinh(4\sqrt{\delta})}\left\{ \begin{array}{l} \dfrac{e^{-4\sqrt{\delta}}}{48\delta}(g_3(t)) - \dfrac{1}{8\sqrt{\delta}}(g_1(t)e^{4\sqrt{\delta}} - g_2(t)e^{-4\sqrt{\delta}}) - \\[2mm] -\dfrac{1}{48\delta}(f_3(t)e^{8\sqrt{\delta}} + g_4(t)e^{-8\sqrt{\delta}}) + \dfrac{g_5(t)}{16\delta}(1-e^{-4\sqrt{\delta}}) \end{array} \right\}$$

$$\lambda(t) = \frac{1}{2\sinh(4\sqrt{\delta})}\left\{ \begin{array}{l} \dfrac{1}{8\sqrt{\delta}}(g_1(t)e^{4\sqrt{\delta}} - g_2(t)e^{-4\sqrt{\delta}}) + \\[2mm] +\dfrac{1}{48\delta}(g_3(t)e^{8\sqrt{\delta}} + g_4(t)e^{-8\sqrt{\delta}}) - \\[2mm] -\dfrac{e^{4\sqrt{\delta}}}{48\delta}(g_3(t) + g_4(t)) - \dfrac{g_5(t)}{16\delta}(1-e^{4\sqrt{\delta}}) \end{array} \right\}$$

# REFERENCES

[1]   Camenschi G. A Mathematical Model of the Permeable Transporting Systems. Rev. Roum. Math. PUres et Appli, Tome XXVIII, Bucarest 1983. 1981; 4: 275-82.

[2]   Fung YC. Biomechanics mechanical properties of of living tissues. Springer Verlag, New York, Inc. 1993.

[3]   Ferguson GG. Physical factors in the initiation, growth, and rupture of human intracranial saccular aneurysms. J Neurosurg 1972; 37: 666-77.
http://dx.doi.org/10.3171/jns.1972.37.6.0666

[4]   Kwembe TA, Jones SN. A mathematical model of cylindrical shaped aneurysms. Biomat 2006, Proceedings of the International Symposium on Mathematical and Computational Biology. Rio de Janeiro, Brazil. world Scientific Publishers 2006; pp. 35-48.

[5]   Sekhar LN, Heros RC. Origgin, growth, and rupture of saccular aneurysms: a review. Neurosurgery 1981; 8: 248-60.
http://dx.doi.org/10.1227/00006123-198102000-00020

[6]   Shah AD, Humphrey JD. Finite strain elastodynamics of intracranial saccular aneurysms. J Biomech 1999; 32: 593-500.
http://dx.doi.org/10.1016/S0021-9290(99)00030-5

[7]   Stehbans WE. Etiology of intracranial berry aneurysms. J Neurysurg 1989; 70: 823-31.

[8]   Steiger HJ. Pathophysiology of development and rupture of cerebral aneurysms. Acta Neurochir Suppl 1990; Wein: 48: 1-57.

[9]   Isaken JG, Bazileus Y, Kuamsdal T, Zhang Y, Kaspersen JH, Waterloo K, Romner B, Ingebrigtsen T. Determination of wall tension in cerebral artery aneurysm by numerical simulation. Stroke 2008; 39: 3172-78.
http://dx.doi.org/10.1161/STROKEAHA.107.503698

[10]  Shojima M, Oshima M, Takagi K, Torii R, Nagata K, Ichiro S, Morita A, Kirino T. Role of the bloodstream impacting force and the local pressure elevation in the rupture of cerebral aneurysms. Stroke 2005; 36: 1933-38.
http://dx.doi.org/10.1161/01.STR.0000177877.88925.06

[11]  Taylor AJ, Bobik A, Berndt MC, Ramsay D, Jennings G. Experimental rupture of artherosclerotic lesions increases distal vascular resistance: A limiting factor to the success of infarct angioplasty. Arterioscler Thromb Vasc Biol 2002; 22: 153-60.
http://dx.doi.org/10.1161/hq0102.101128

[12]  Michel CC, Curry FE. Microvascular Permeability. Physiol Rev 1999; 79: 703-61.

[13]  Moftaker R, Aagaard-Kienitz B, Johnson K, Turki PA, Turk AS, Niemann DB, Consigny D, Grinde J, Wiebeno, Mistretto CA. Noninvasive Measurement of Intra-aneurysmal Pressure and Flow Pattern using Phase Contrast With Vastly Undersampled Isotropic Projection Imaging. AJNR Am J Neuroradiol 2007; 28: 1710-14.
http://dx.doi.org/10.3174/ajnr.A0648

[14]  Darcy H. Les Fontaines Publiques de la ville de Dijon, Dalmont, Paris 1856.

[15]  Lee T, Lakes RS. Anisotropic polyurethane foam with Poisson's ratio greater than 1. J Mater Sci 1997; 32: 2397-401.
http://dx.doi.org/10.1023/A:1018557107786

[16]  Mazumdar J. An introduction to mathematical physiology and biology, 2nd ed. New York 1999; pp. 136-161.
http://dx.doi.org/10.1017/CBO9781139173278.010

[17]  Benderson J, Connolly E, Batjer H, *et al*, Guidelines for the management of aneurysmal subarachnoid hemorrhage: a statement for healthcare professionals from a special writing group of the Stroke Council, American Heart Association. Stroke 2009; 40(3): 994-1025.

[18]  Ting TCT, Chen T. Poisson's ratio for anisotropic elastic materials can have no bounds. Q J Mechanics Appl Math 2005; 58(1): 73-82.

[19]  Brisman JL, Song JK, Newell DW. Cerebral aneurysms. N Engl J Med 2006; 355(9): 928-39.

[20]  Greaves GN, Greer AL, Lakes RS, Rouxel T. Poisson's Ratio and Modern Materials. Nat Mater 2011; 10: 823-36.
http://dx.doi.org/10.1038/nmat3134

[21]  Lakes RS, Wineman A. On Poisson's Ration in Linearly Viscoelastic Solids. J Elasticity 2006; 85: 45-63.
http://dx.doi.org/10.1007/s10659-006-9070-4

[22]  Norris AN. Extreme values of Poisson's ratio and other engineering moduli in anisotropic materials. J Mechan Mater Struct 2006; 1(4): 793-12.

[23]  Olafsson E, Hauser WA, Gudmundsson G. A population-based study of prognosis of ruptured cerebral aneurysm: mortality and recurrence of subarachnoid hemorrhage. Neurology 1997; 48(5): 1191-95.

[24]  West J. Respiratory Physiology: the essentials – 9th edition. Baltimore: Lippincott Williams & Wilkins 2012; p. 177.

[25]  Michel CC. Fluid exchange in the microcirculation. Physiol 2004; 557(3): 701-702.

[26]  Michel CC. Microvsular permeability, ultrafiltration, and restricted diffusion. Am J Physiol Heart Circ Physiol 2004; 287: H1887-H1888.
http://dx.doi.org/10.1152/classicessays.00012.2004

[27]  Fick A. Annalen der Physik 1855; 170(1): 59-86.

[28]  Nagy JA, Benjamin L, Zeng H, Dvorak AM, Dvorak HF. Vascular permeability, vascular hyperpermeability, and angiogenesis. Angiogenesis 2008; 11: 109-19.
http://dx.doi.org/10.1007/s10456-008-9099-z

[29]  Sample C, Golovin AA. Morphological and chemical oscillations in a couple-membrane system. SIAM J Appl Math 2011; 71: 622-34.
http://dx.doi.org/10.1137/100800154

[30]  Sample C, Golovin AA. Nonlinear dynamics of a double bilipid membrane. Phys Rev E 2007; 76: article 031925.

[31] Kyriacou SK, Humphrey JD. Influence of size, shape and properties on the mechanics of axisymmetric saccular aneurysms. J Biomech 29(8): 1996; 1015-22.

[32] Milnor WR. Hemodynamics. Williams & Wilkens, Baltimore 1982.

[33] Bender CM, Orszag SA. Advanced mathematical methods for scientists and engineers. McGraw Hill, Inc. 1978; pp. 319-361.

[34] Segers P, Carlier S, Pasquet A, Rabben SI, Hellevik IR, Remme E, De Backer T, De Sutter J, Thomas JD, Verdonck P. Individualizing the aorta-radial pressure transfer function: feasibility of a model based approach. Am J Physiol Heart Circ Physiol 2000; 279: H542-H549.

[35] Greenberg MS. Subarachnoid hemorrhage and aneurysms. In: Greenberg, M.S, ed. Handbook of Neurosurgery, 5th ed. Thieme Medical Publishers, Newy York 2001; pp. 754-803.

[36] Morey SS. AHA recommendations for the management of intracranial aneurysms. Agency for Health Care Policy and Research. Am Fam Physician 2001; 63(12): 2465-66.

[37] Fisher CM, Kristler JP, Davis JM. Relation of cerebral vasospasm to subarachnoid hemorrhage visualized by computerized tomographic scanning. Neurosurgery 1980; 6(1): 1-9.

[38] Barker FG, Ogilvy CS. Efficacy of Prophylactic nimodipine for delayed ischemic deficit after subarachnoid hemorrhage: a metaanalysis. J Neurosurgery 1996; 84(3): 405-14.

[39] Evans E, Mohandas N, Leung A. Static and Dynamic Rigidities of Normal and Sickle Erythrocytes: Major Influence of Cell Hemoglobin Concentration. J Clin Invest 1984; 73: 477-88.
http://dx.doi.org/10.1172/JCI111234

[40] Mohandas N, Evans E. Mechanical Properties of the red cell membrane in relation to Molecular Structure and Genetic defects. Annu Rev Biophys Biomol Struct 1994; 23: 787-18.
http://dx.doi.org/10.1146/annurev.bb.23.060194.004035